NASA CONTRACTOR REPORT

NASA CR-151974

(NASA-CR-151974) FORMATION FLYING BENEFITS BASED ON VORTEX LATTICE CALCULATIONS (Analytical Methods, Inc., Bellevue, Wash.) 58 p HC A04/MF A01 CSCL 01A

N77-20020

Unclas G3/02 22617

FORMATION FLYING BENEFITS BASED ON VORTEX LATTICE CALCULATIONS

by Brian Maskew

Prepared by
ANALYTICAL METHODS, INC.
Bellevue, Washington 98004
for Ames Research Center

NATIONAL AERONAUTICS AND SPACE ADMINISTRATION • WASHINGTON, D. C.

FOREWORD

The research reported here was performed under Purchase Order A-26151-B(DG) between Analytical Methods, Inc., Belleview, Washington, and the National Aeronautics and Space Administration. The NASA project monitor was Remus N. Bretoi, who also prepared Appendix A. The AMI principal investigator was Brian Maskew.

ABSTRACT

A quadrilateral vortex-lattice method was applied to a formation of three wings to calculate force and moment data for use in estimating potential benefits of flying aircraft in formation on extended range missions, and of anticipating the control problems which may exist. The investigation led to two types of formation having virtually the same overall benefits for the formation as a whole, i.e., a "V" or echelon formation and a double row formation (with two staggered rows of aircraft). These formations have unequal savings on aircraft within the formation, but this allows large longitudinal spacings between aircraft which is preferable to the small spacing required in formations having equal benefits for all aircraft. A reasonable trade-off between a practical formation size and range benefit seems to lie at about three to five aircraft with corresponding maximum potential range increases of about 46% to 67%. At this time it is not known what fraction of this potential range increase is achievable in practice.

CONTENTS

	Page
SUMMARY	1
INTRODUCTION	2
LIST OF SYMBOLS	3
CALCULATION METHOD	4
BASIC DATA	8
RESULTS AND DISCUSSION	14
OPTIMUM FORMATIONS	31
RANGE EXTENSION	35
CONCLUSIONS AND RECOMMENDATIONS	38
REFERENCES	40
APPENDIX A	A-1

FIGURES

		Page
1.	Vortex-lattice Arrangement and Formation Definition . . .	8
2.	Summary of Formation Positions Considered	9
3.	Lift and Induced Drag Characteristics for Wing Alone . .	12
4.	Effect of Streamwise Position: z/b = 0.0; y/b = 0.89 (except y/b = 1.0 at x/b = 0.0).	15
5.	Effect of Spanwise Position: x/b = 3; z/b = 0.0.	19
6.	Effect of Spanwise Position: x/b = -3; z/b = 0.0	22
7.	Effect of Vertical Position: x/b = 3; y/b = .89	24
8.	Effect of Vertical Position: x/b = -3; y/b = .89	27
9.	Spanwise Distributions of Lift and Induced Drag: x/b = 3; y/b = .98; z/b = 0.	29
10.	Upwash Induced by a Semi-infinite Vortex	32
11.	Possible Formations	33
12.	Relative Range Versus Number of Aircraft in Formation	37

TABLES

		Page
1.	Basic Wing Geometry	10
2.	Relative Range Vs. Number of Aircraft in Formation . . .	37
3.	A-1. Relative Range as a Function of Number of Aircraft In Formation	A-12

FORMATION FLYING BENEFITS

BASED ON VORTEX-LATTICE CALCULATIONS

Brian Maskew*

SUMMARY

A quadrilateral vortex-lattice method was applied to a formation of three wings to calculate the force and moment data for use in estimating potential benefits of flying aircraft in formation on extended range missions, and of anticipating the control problems which may exist.

The investigation led to two types of formation having virtually the same overall benefits for the formation as a whole. Calculations indicate that "V" or echelon formations have an induced drag reduction of 80% on all but the leading aircraft. Double-row formations (with two staggered rows of aircraft) have virtually no induced drag savings in the leading row, but aircraft in the second row have an induced thrust of 48% of their free-air induced drag. Both formations have large longitudinal distances between aircraft (about three wing spans), and are, therefore, preferable to formations having equal benefits for all aircraft. The latter formations require vary small spacings as observed in migrating bird formations. The double-row formation has an advantage over the "V" formation in that rolling moment required for trim is zero. Both formations are insensitive to longitudinal spacing, but benefits (and trimming problems) decrease rapidly with lateral and vertical movements from the optimum locations.

A reasonable trade-off between a practical formation size and range benefit seems to lie at about three to five aircraft with corresponding maximum potential range increases of about 46% to 67%. At this time it is not known what fraction of this potential range increase is achievable in practice.

The optimum locations require the trailing vortices from the leading wings to pass close to the tips of the followers, and this poses a problem for existing calculation techniques. The problem affects not only the prediction of the maximum benefits, but also the stability and control aspects of holding formation. Further work, therefore, is recommended to investigate force and moment calculations with close vortex/wing interactions and to refine the calculation method. The results should then be used to analyse the control, stability and range performance of specific aircraft in formation.

---

*Senior Research Scientist, Analytical Methods, Inc., Bellevue, Washington

INTRODUCTION

Recently there has been renewed interest in the concept of flying aircraft in formation to increase their range or to reduce the amount of fuel required for a given range. Modern avionics and control augmentation systems (including alternative autopilot modes) would facilitate holding accurate formation positions over long periods and would thereby help to achieve the maximum benefits. The benefits arise from an induced drag saving that is caused by favorable aerodynamic interference between the aircraft. So far, formation flying calculations, such as references 1 through 4, have been based mainly on a simple horseshoe vortex representation of each wing; Shollenberger's calculations (ref. 4), however, indicate important differences between the results from that simple approach and from one based on elliptic loading when the spanwise spacing between wing tips is less than about a semispan. In fact, significant benefits are obtained only with spanwise spacings considerably smaller than a wing semispan, and so a detailed wing representation is clearly required for accurate calculations. This requirement is especially important in practical calculations in which each aircraft is trimmed in roll. Formations considered in previous calculations were mainly based on achieving the same induced drag saving for each aircraft in the formation -- a situation that evidently exists in migrating bird formations. For aircraft, however, such formations require dangerously small spacings.

The present objective is to apply a vortex-lattice method (ref. 5) to calculate formation flying benefits and to consider a range of formations to find safer alternatives to the "equal benefits" formation. Use of the vortex-lattice method allows a more realistic calculation than is possible with the simple horseshoe-vortex model; the mutual interference effects can be represented in greater detail, and each wing can be trimmed in roll. The main aims of this study are to find optimum formation configurations to assess the loss in benefits caused by small movements from the optima, and to assess the degree of sensing and control required to maintain range benefits within given limits. The wing planform used in the calculation is based on a possible military S.T.O.L. transport aircraft configuration.

LIST OF SYMBOLS

x, y, z	Cartesian coordinate system (see fig. 1)
C_L	lift coefficient = lift/(q_∞s)
C_{D_i}	induced drag coefficient = induced drag/(q_∞s)
C_ℓ	rolling moment coefficient = rolling moment/(q_∞sb)
q_∞	free-stream dynamic pressure
V_∞	true air speed of formation, m/s
S	wing planform area, m^2
α	wing incidence relative to the flight vector, deg.
ξ	flaperon deflection, positive downwards, deg.
b	wing span, m

Subscripts:

A	inner wing	See figure 1
B	outer wing	See figure 1
S	single	
F	formation	

CALCULATION METHOD

Basic Method

The method (ref. 5) used here is based on vortex-lattice theory (e.g., ref. 6), but the wing lattice is formed into quadrilateral vortices (fig. 1) instead of horseshoe vortices. Each quadrilateral has a control point at which the boundary condition of zero normal velocity is specified; the normal velocity includes a component of the free-stream velocity and contributions from all the trailing vortices and quadrilateral vortices in the lattices (i.e., on all the wings in the formation in this case). This gives a set of simultaneous equations in the unknown quadrilateral-vortex strengths; for example,

$$\frac{1}{4\pi}\Gamma_k A_{jk} + B_j = 0; \qquad j = 1, \ldots, N \quad k = 1, \ldots, N \tag{1}$$

where Γ_k is the k^{th} quadrilateral-vortex strength,

A_{jk} is the influence coefficient for the normal component of velocity (ref. 5) induced at the j^{th} quadrilateral control point by the k^{th} quadrilateral vortex;

B_j is the normal component of free-stream velocity at the j^{th} control point; and

N is the total number of quadrilateral vortices in the system.

Initially, the trailing vortices are assumed semi-infinite in the streamwise direction, but the method incorporates an iterative procedure for calculating the trajectories of the vortices for a force-free wake. In this procedure, the first part of each trailing vortex is divided into a number of short, straight segments, and each segment is aligned with the local mean velocity vector. As the wake geometry changes, the trailing vortex contributions to the coefficients, A, in Equation (1) change, and so a new vortex strength solution is calculated at each iteration.

For most of the present calculations, the procedure was terminated at the end of the first pass, i.e., with the straight undeflected wake. One case was attempted with the wake iteration to assess the effect of wake roll-up.

When the quadrilateral vortex strengths are known, the forces and moments are calculated by applying the Kutta Joukowski law to each bound vortex segment in the lattices, viz.:

$$\underline{C}_f = \frac{2\underline{V}\wedge\underline{s}\Gamma}{SV_\infty^2} \tag{2}$$

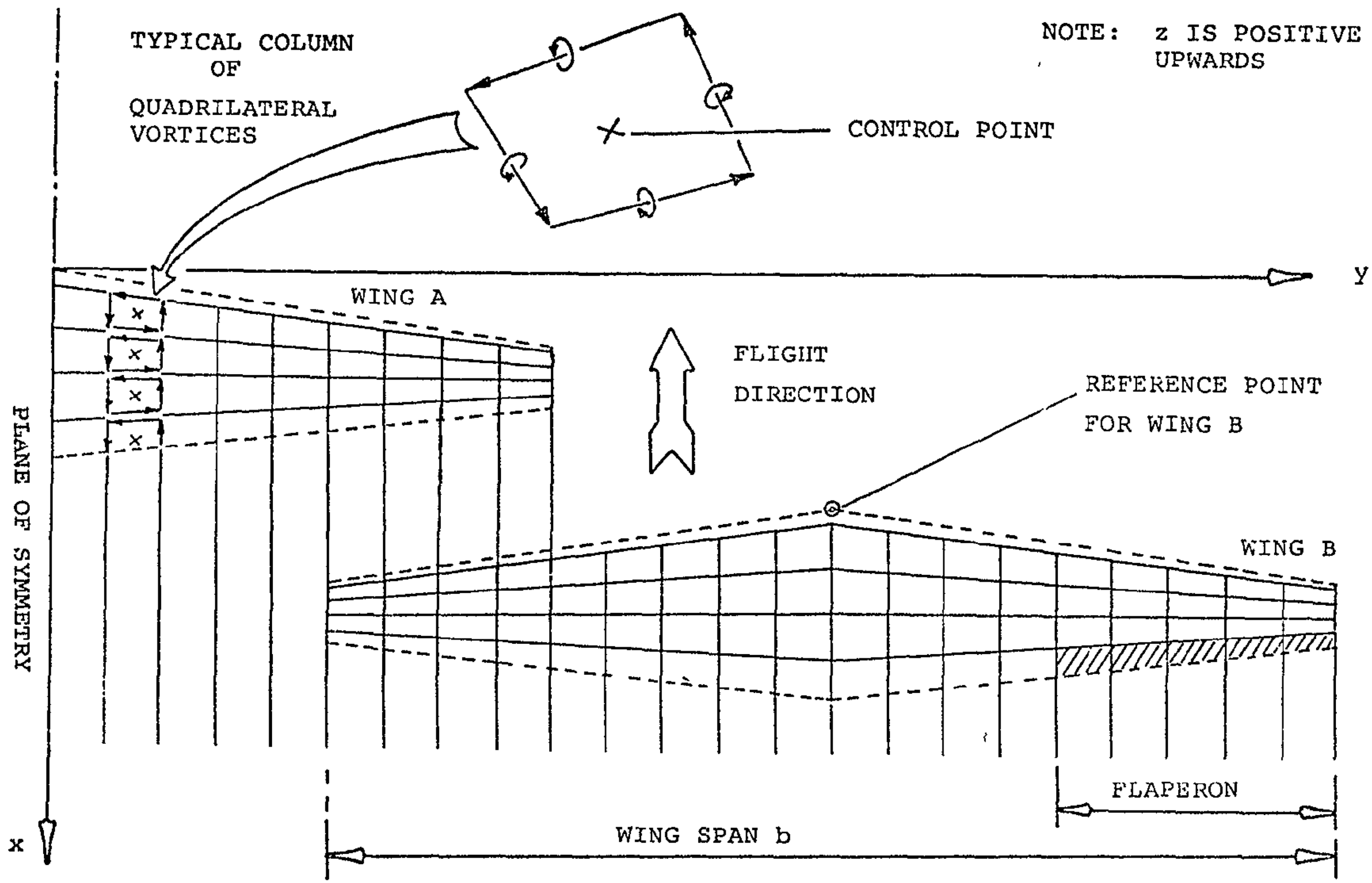

Figure 1. Vortex-lattice Arrangement and Formation Definition.

where $\underline{C}_f$ is the force vector coefficient which is resolved into the lift and drag direction;

$\underline{V}$ is the calculated local velocity vector at the bound vortex segment mid-point; and

$\underline{s}$ is the vortex segment vector.

The force is assumed to act at the segment mid-point for the purpose of evaluating moments.

Formation Representation

Symmetrical formations are assumed; this halves the total number of unknown quadrilateral vortex strengths for a given problem. The formations consist of three wings and each wing has a lattice of 4 (chordwise) by 18 (spanwise) quadrilaterals, figure 1. The total number of unknowns, therefore, is 108.

Ideally, more quadrilateral elements should be used, e.g., 6 x 30 on each wing, but the computer program is limited to 150 unknowns and 30 trailing vortices at this time. Also, the lattice should be set in from each wing tip by a quarter of a quadrilateral "span" for best results (ref. 5); in the program coding prevented this from being applied directly on the inner tips of the outer wings, and so tip inset was not used in these calculations. Because the main interest in this study is in ratios of induced drag, etc., (i.e., formation values/free-air values) rather than absolute values, neither of the above factors will be a serious drawback to the present calculations.

Trimming Procedure

Each wing is trimmed in pitch so that all the wings in the formation have the required lift coefficient, C_L. The outer wings are also trimmed in roll using a downward-deflecting "flaperon" (fig. 1). It is assumed that the flap mechanism could be arranged to allow the flaps on one side only to be deflected to provide the basic asymmetry required in some of the formations; the aileron would be treated similarly, and would be used for periodic trimming purposes to maintain formation position.

In the calculations, the wings are set initially at incidence α (i.e., $\alpha_A = \alpha_B = \alpha$) giving the required lift coefficient in free-air conditions, and the outer wings have zero flaperon deflection, i.e., $\xi_B = 0$. The initial solution gives lift coefficients C_{L_A} and C_{L_B} for the inner and outer wings, respectively, and an out-of-balance rolling moment, C_{ℓ_B}, for the outer wings. Using superscripts o and n for the old and new conditions, respectively, the trimmed incidence for wing A is approximately:

$$\alpha_A^n = \alpha_A^o + (C_L - C_{L_A}^o) \Big/ \frac{dC_L}{d\alpha} \tag{3}$$

where the lift curve slope, $\frac{dC_L}{d\alpha}$, is calculated for a single wing with the same vortex lattice.

For the outer wing, the flaperon is first deflected through angle ξ_B to trim out the rolling moment:

$$\xi_B^n = -C_{\ell_B}^o \Big/ \frac{dC_\ell}{d\xi} \tag{4}$$

Because of asymmetry, the deflected flaperon gives a lift increment. The trimmed incidence for wing B, therefore, is approximately:

$$\alpha_B^n = \alpha_B^o + (C_L - C_{L_B}^o - \frac{dC_L}{d\xi} \cdot \xi_B^n) \Big/ \frac{dC_L}{d\alpha} \tag{5}$$

The trimming steps are repeated until the C_L value and zero rolling moment are achieved.

BASIC DATA

Wing Geometry

Figure 1 shows the wing planform including the flaperon. The basic details are given in table 1. For one calculation the flaperon span was extended over the full semispan.

Formations

The coordinate system for defining the formations is shown in figure 1, and figure 2 shows a summary of the formations considered. Wing A, the inner wing, is fixed at the origin, while Wing B (and its image) moves along five scan lines, one streamwise, two spanwise and two vertical. The streamwise scan is in the plane $z = 0$, and goes from three spans upstream of the origin to three spans downstream. Except for one case where all three wings are tip to tip, the spanwise position of Wing B in the streamwise scan is at $y/b = 0.89$; this places the tip of the following wing near to the centroid of shed vorticity from the leading wing semispan.

There are two spanwise scans in the plane $z = 0$, one at three spans upstream of the origin and one at three spans downstream. Spanwise positions range from $y/b = 0.83$ to 2 in each scan.

There are two vertical scans, one at three spans upstream and the other at three spans downstream of the origin. These scans include the common points in the streamwise and spanwise scans, viz., $y/b = 0.89$. The vertical movement from $z = 0$ is 0.5b.

In formations where the trailing vortex-lattice from the leading wing overlaps the lattice on the following wing, (i.e., formations with $y/b < 1$) a numerical problem occurs in the calculations if the lattices do not match (ref. 7); only spanwise positions which line up the lattices are therefore considered (see fig. 1).

Single Wing Aerodynamic Characteristics

Figure 3 shows the basic lift and induced drag characteristics calculated for a single wing represented by the 4 x 18 lattice. Because of the limitations mentioned under "Formation Representation", these characteristics should be regarded as approximate in the absolute sense; they are used for trimming the calculations here and for the base in the ratio between formation and free-air conditions. (However, a calculation was made at $\alpha = 7°$ with a tip inset of a quarter quadrilateral span and a 4 x 40 lattice, i.e., a 4 x 20 lattice on

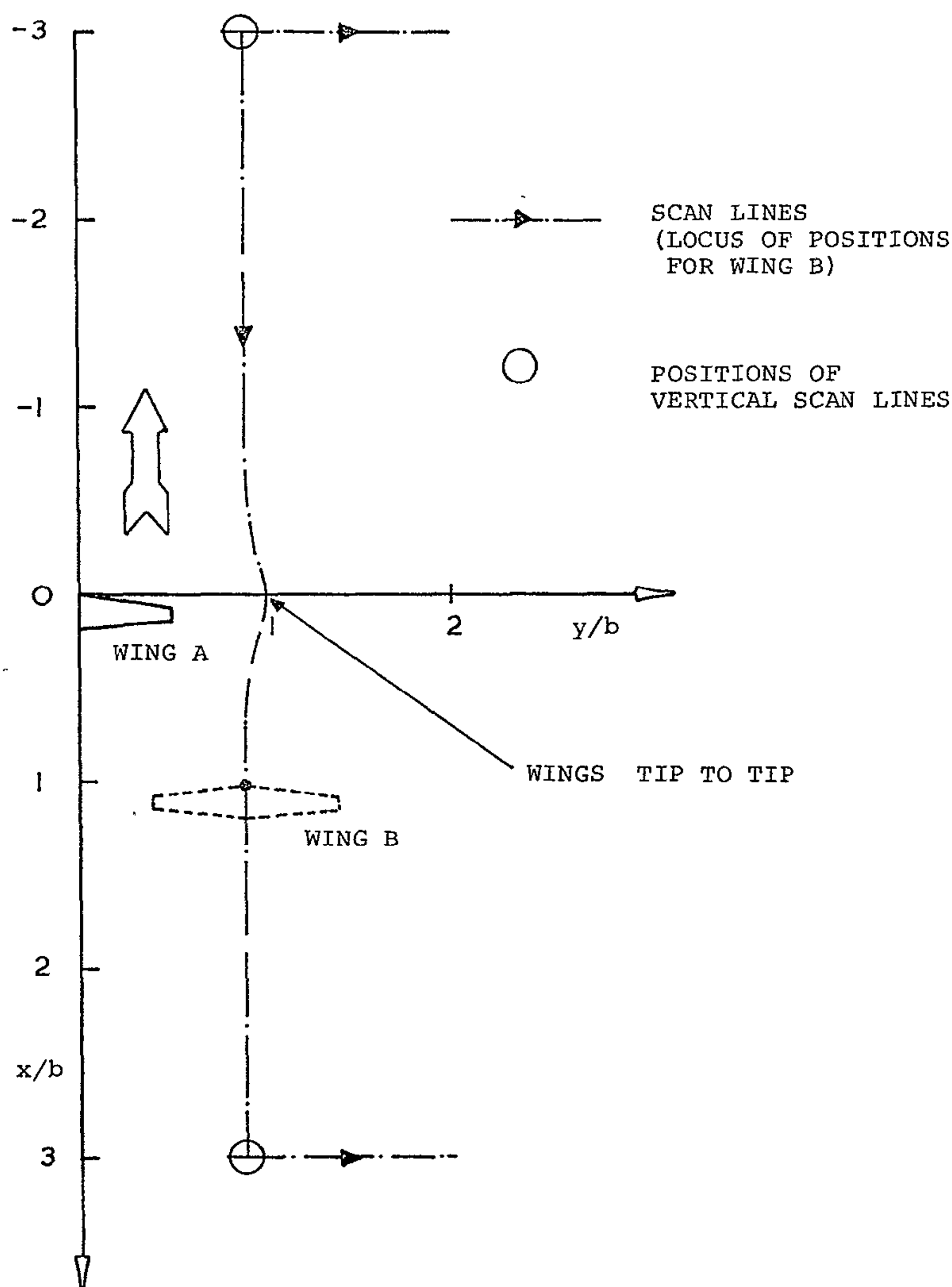

Figure 2. Summary of Formation Positions Considered.

Table 1. Basic Wing Geometry
(Based on a Semispan of 1.0)

span	2.0
geometric mean chord	0.25
area	0.5
aspect ratio	8.0
taper ratio	0.33
sweepback (quarter-chord line) . . .	5°
dihedral	0
twist	0
flaperon span	0.44 to 1.0
flaperon chord/local chord	0.19

the half span. The results (fig. 3) show only a small displacement from the 4 x 18 lattice characteristics.)

The lift curve slope to be used in equations (3) and (5) is, therefore:

$$\frac{dC_L}{d\alpha} = 0.0851 \text{ per degree} \tag{6}$$

The flaperon effectiveness (for equations (4) and (5)) calculated at $\alpha = 0$ with the 4 x 18 lattice is:

$$\left.\begin{aligned} \frac{dC_\ell}{d\xi} &= 0.002982 \text{ per degree} \\ \frac{dC_L}{d\xi} &= 0.01060 \text{ per degree} \end{aligned}\right\} \tag{7}$$

(The corresponding quantities calculated with a 4 x 20 lattice were 0.003014 and 0.01065, respectively. Because of asymmetry, this calculation considered the full wing and the lattice was, therefore, limited by the number of trailing vortices allowed in the computer program, viz., 30 at this time.)

Data Points

Calculations performed for each formation configuration (after trimming) evaluate the induced drag for each wing and for the formation, together with the incidence (for the required lift coefficient) and the flaperon angle. The induced drag and the incidence are then divided by the corresponding free-air values (at the same C_L). The single-wing data are:

for $C_L = 0.6$,

$$C_{D_i} = 0.01296$$

$$\alpha = 7.051°$$

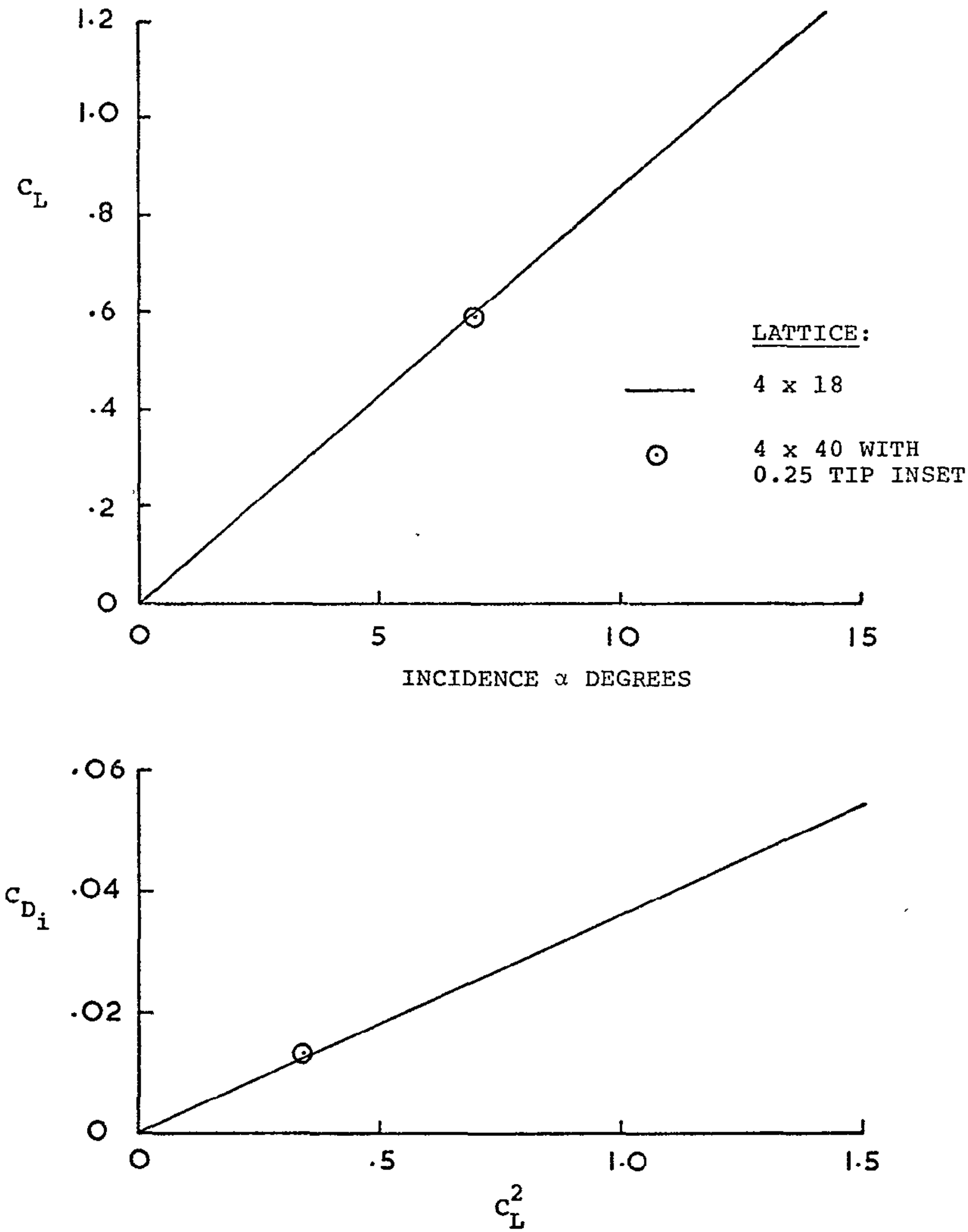

Figure 3. Lift and Induced Drag Characteristics for Wing Alone.

and for $C_L = 1.2$,

$$C_{D_i} = 0.05189$$

$$\alpha = 13.92°$$

(Both sets of data are for the 4 x 18 lattice.)

A few data cases considered at the higher C_L values gave essentially the same incidence and induced drag ratios as for the $C_L = 0.6$ case because of the approximate linear relationships of $C_L \sim \alpha$ and $C_{D_i} \sim C_L^2$ (fig. 3).

The incidence and flaperon angles for each formation are related back to approximate lift and rolling moment increments, respectively (using the derivatives from equations (6) and (7)). These quantities vary approximately linearly with C_L and are presented divided by the C_L value of the calculation (i.e., 0.6).

RESULTS AND DISCUSSION

Streamwise Scan

Figure 4(a) shows the induced drag ratio variations as wing B (and its image) moves from three spans upstream to three spans downstream of wing A. The corresponding variations in incidence ratio, lift increment, flaperon angle and rolling moment are given in parts (b), (c) (d) and (e) of figure 4, respectively.

The position for equal induced drag benefit for all three wings occurs at a very small x/b value, i.e., 0.15, giving a streamwise distance of approximately 1.5 tip chords between the tip trailing-edge of wing A and the tip leading-edge of wing B.

The induced drag ratio for the formation of three wings remains virtually constant at 0.468 over the complete scan (and therefore complies with Munk's stagger theorem). The individual wing induced drag values change markedly in the region where wings A and B change place as leader, but, by three spans upstream and downstream of the origin, the values have almost reached steady conditions. Wing B achieves an induced drag ratio of 0.21 at x/b = 3.0; the limiting value is 0.20 for the larger downstream distances assuming the total for the three wings remains constant and that wing A goes to free-air conditions.

At x/b = -3, wing B has an induced drag ratio of 0.94, but wing A is now in an upwash field from both wings B and receives a negative induced drag ratio (i.e., a thrust) of -0.48.

The angle of incidence for a given C_L is reduced appreciably in formation, figure 4(b). The incidence ratio for wing B is 0.83 at x/b = 3 while that for wing A with x/b = -3 goes down to 0.767. The corresponding lift increment ratios (before trimming) are 0.127 and 0.235 respectively (fig. 4(c)).

The flaperon angle required to trim the rolling moment on wing B is 2.7° when x/b = 3 (fig. 4(d)), and represents an induced rolling moment coefficient of $-0.0133C_L$ (fig. 4(e)). Formations with wings B ahead of wing A have almost negligible rolling moment.

One case was considered at x/b = 3 with a full semispan flaperon to see if this would reduce the roll trim drag. The larger flaperon, rather than reducing trim drag, gives a small increase (fig. 4(a)). (But the smaller deflection required by the larger flaperon should reduce any profile drag penalty.) Evidently, deflecting the shorter flaperon must have improved the basic loading distribution towards the ideal elliptical shape, giving a <u>negative</u> trim drag for this wing. Deflecting the larger flaperon essentially restored the basic loading distribution and induced drag.

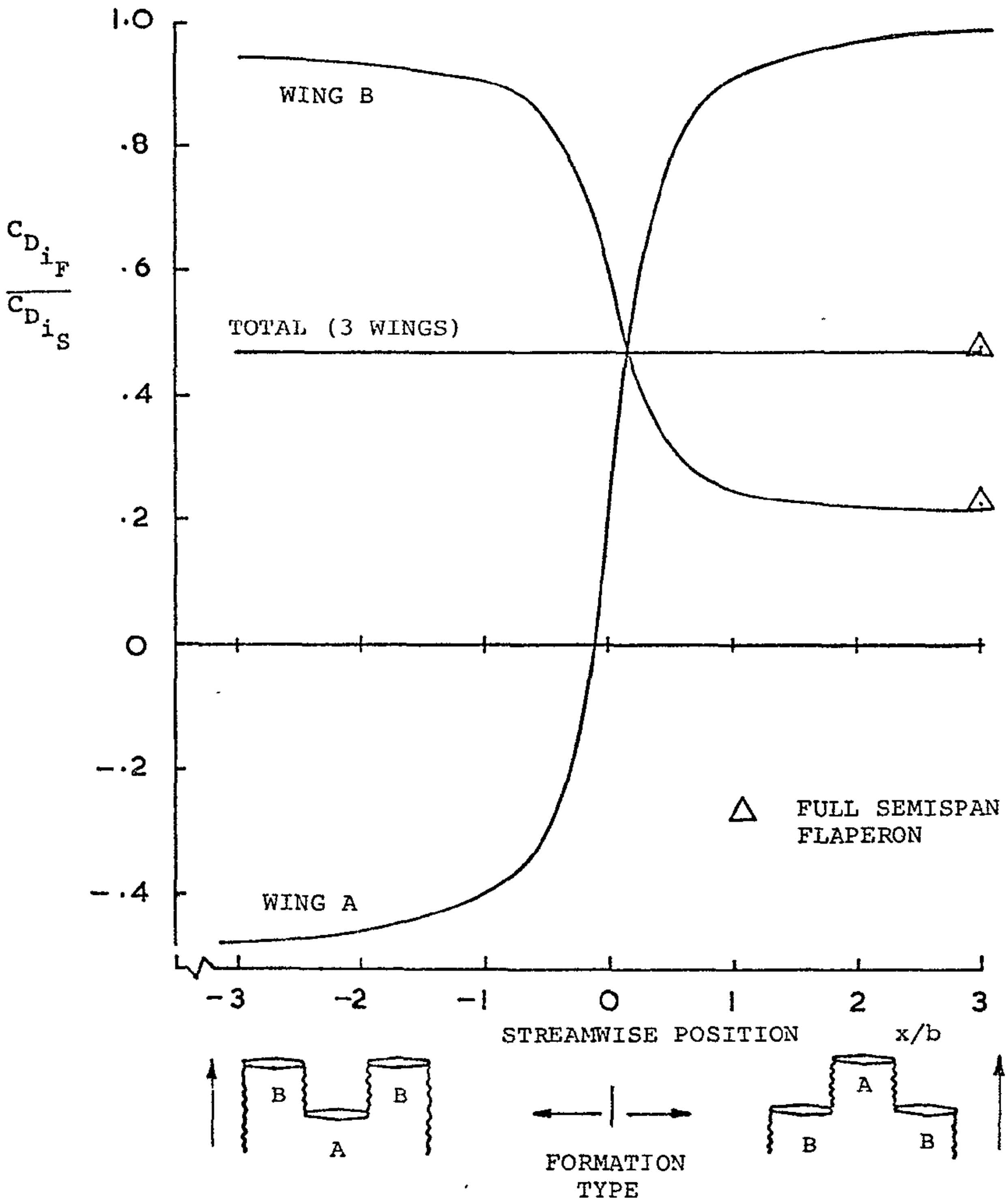

(a) Induced Drag Ratio.

Figure 4. Effect of Streamwise Position: $z/b = 0.0$; $y/b = 0.89$ (except $y/b = 1.0$ at $x/b = 0.0$).

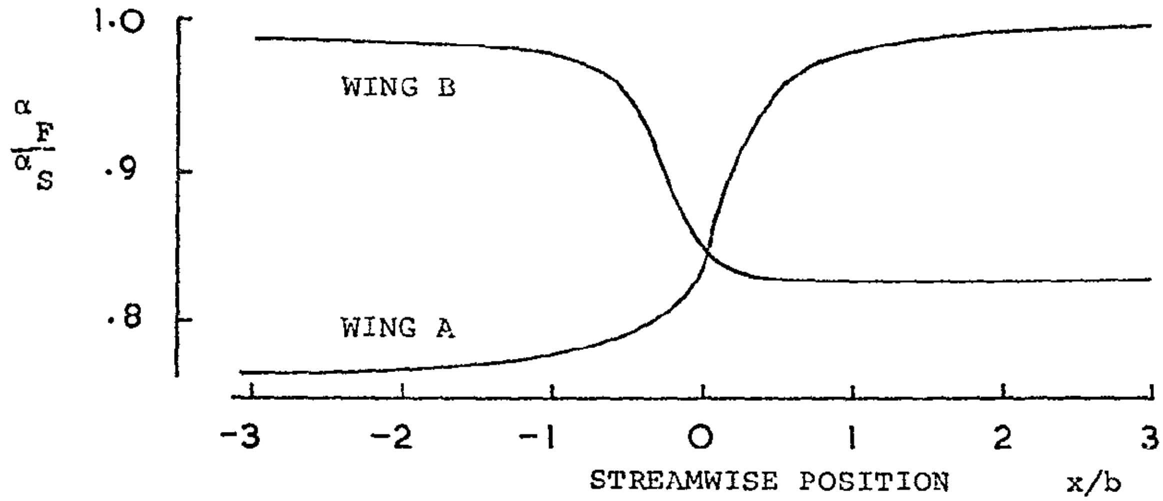

(b) Incidence Ratio.

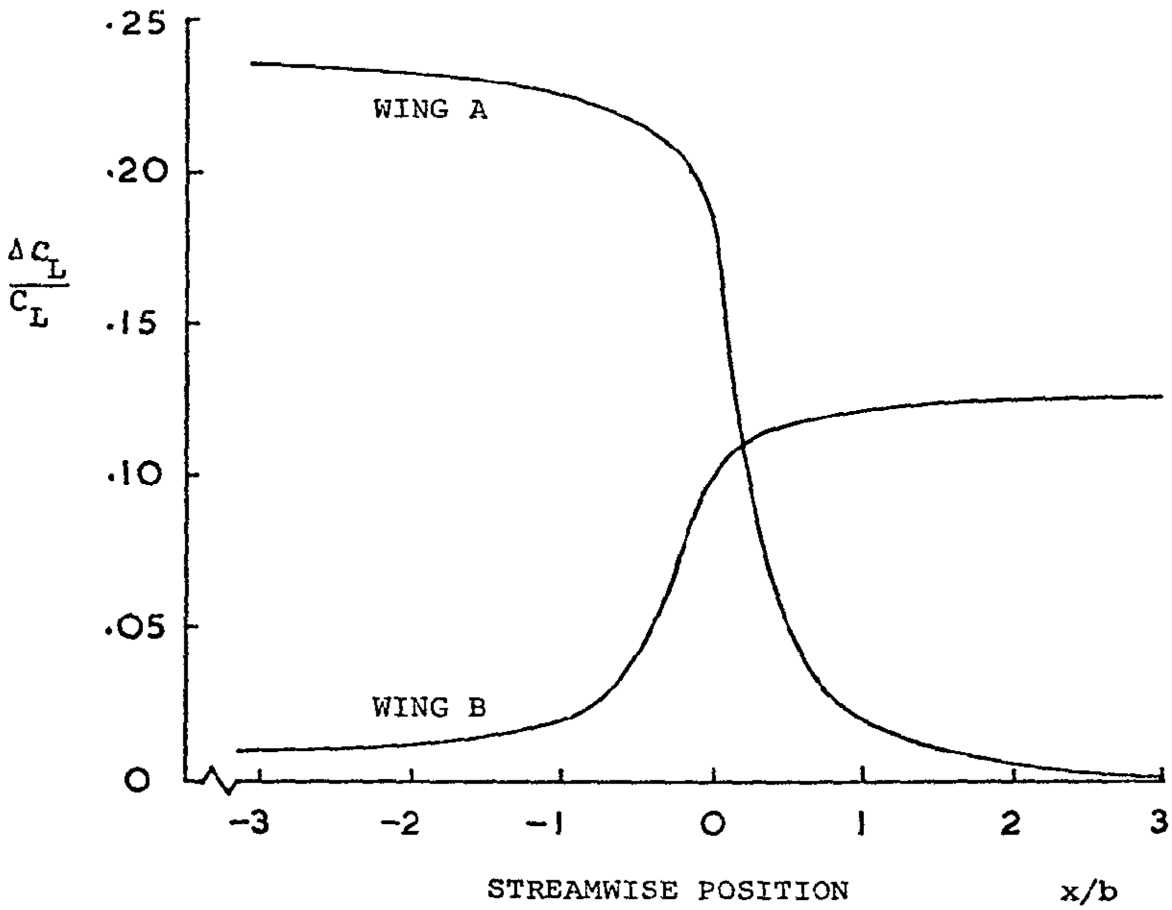

(c) Lift Increment in Formation.

Figure 4. Continued.

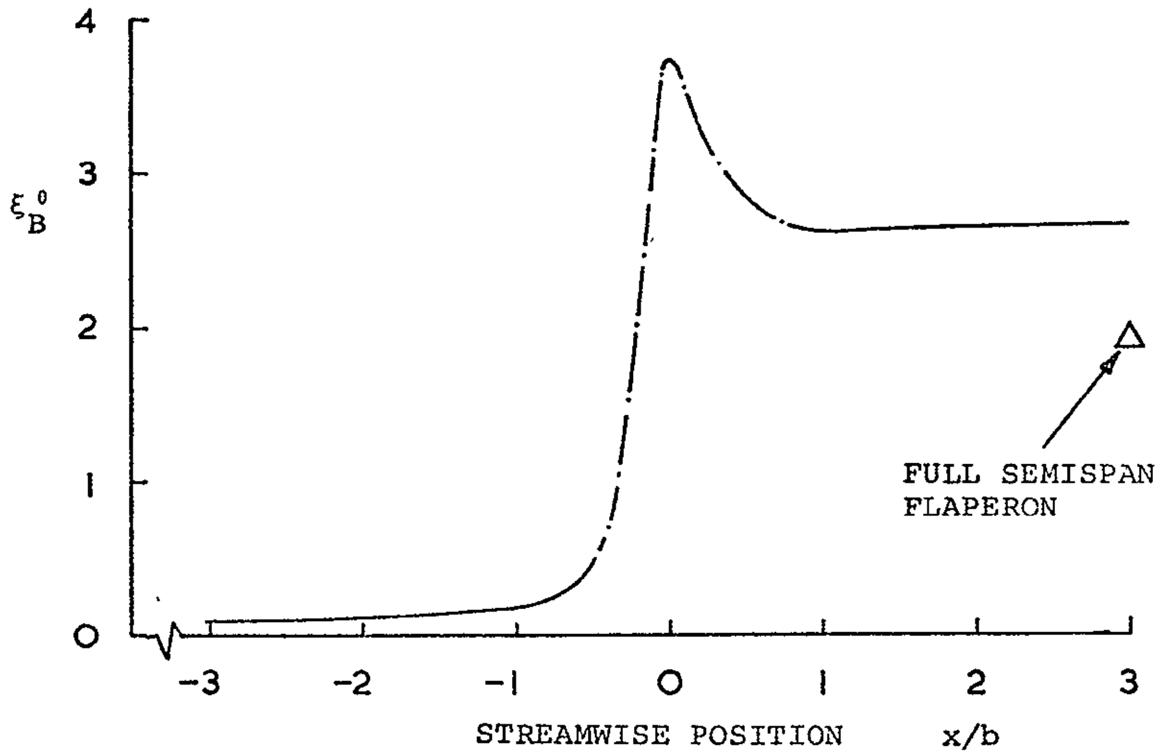

(d) Flaperon Deflection.

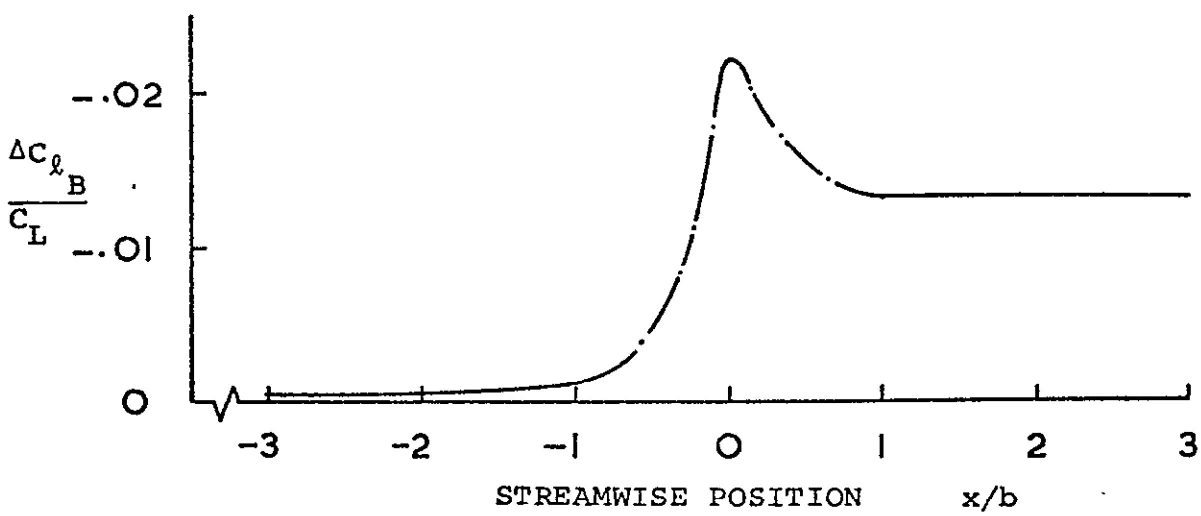

(e) Rolling Moment Increment in Formation.

Figure 4. Concluded.

Spanwise Scans

The induced drag ratio variation with spanwise movement at x/b = 3 is shown in figure 5(a) for wings A and B and for the formation of three wings. The minimum value of 0.21 for wing B at the spanwise position of 0.89 (fig. 4(a)) increases to 0.28 at y/b = 1.0, then increases rapidly and is 0.49 at y/b = 1.05. The variations in the incidence, induced lift, flaperon angle and rolling moment ratios, figure 5(b), (c), (d) and (e), respectively, become very steep as y/b decreases towards 1; i.e., as the inner tip of wing B approaches the edge of wing A's trailing lattice. As y/b increases from 1.0 to 1.05, the incidence ratio increases by 0.07 (fig. 5(b)), the induced lift decreases by $0.037C_L$ (fig. 5(c)), and the induced rolling moment decreases by $0.01C_L$ (fig. 5(e)). The rapid turnover that occurs near y/b = 1 is a limitation of the lattice approach at this time, and is discussed later under "Effect of Wake Roll-Up".

This formation is roll stable, i.e., with flaperon fixed in a trimmed position, a spanwise movement of wing B would cause changes in induced rolling moment that would tend to return the wing to the trimmed conditon. The results for the spanwise scan with wing B at x/b = -3 are shown in figure 6. The induced drag ratio for wing A (fig. 6(a)) shows a rapid variation from the thrust value seen in figure 4(a); as y/b increases from 1.0 to 1.05 the ratio increases by 0.46. The kink at y/b = 1.0 seen in figure 4(a) for wing B is present here also for wing A.

The incidence and induced lift ratios for wing A (figs. 6(b) and (c)) also have rapid variation near y/b = 1.0; as wing B moves from y/b = 1.0 to 1.05, the incidence ratio for wing A increases by 0.07 and the corresponding induced lift decreases by .068 C_L

The rolling moment on wing B is not plotted for this case; the maximum flaperon deflection calculated at x/b = -3 is about 0.1°.

Vertical Scans

The results for a vertical scan at x/b = 3.0, y/b = 0.89, are given in figure 7. These show a strong sensitivity to vertical movement. The 0.21 induced drag ratio for wing B (fig. 4(a)) increases to 0.35 for a vertical movement of 0.05b, see figure 7(a). The incidence ratio, meanwhile, increases by 0.04 (fig. 7(b)) and the induced lift ratio, $\Delta C_L/C_L$, decreases by 0.025 (fig. 7(c)).

The formations considered here keep the following wings (i.e., wing B) above the wake of the leader. This is stable as far as lift is concerned, ie.e, a vertical displacement upwards would reduce the induced lift, (fig. 7(c)), causing the wing to come back down, and vice-versa. With wing B below the wake, a downward displacement would reduce the induced lift and so the wing would continue going down.

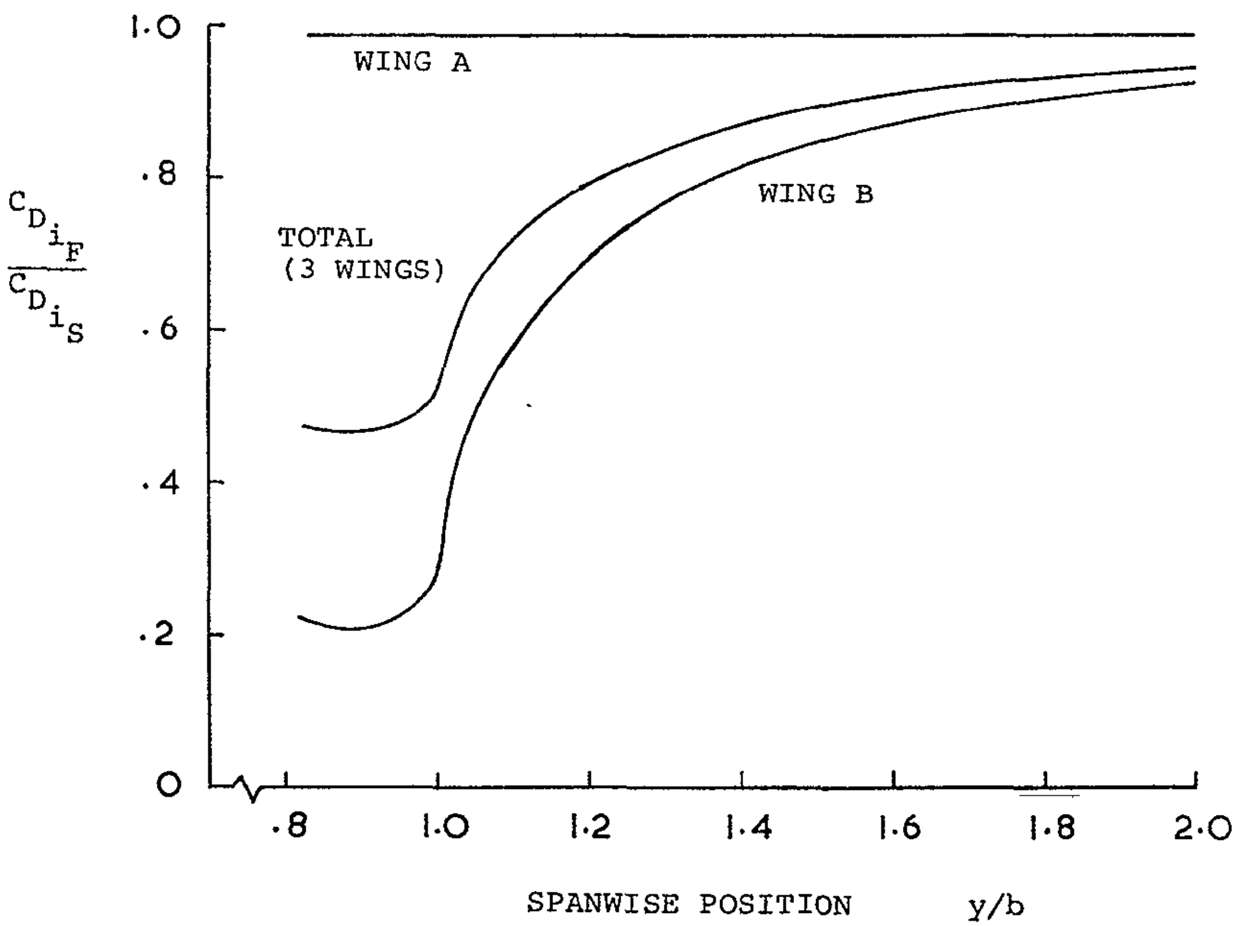

FORMATION
TYPE

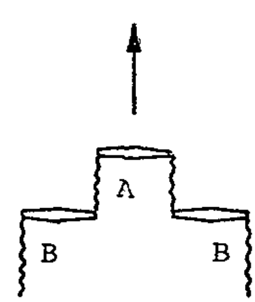

(a) Induced Drag Ratio.

Figure 5. Effect of Spanwise Position: $x/b = 3$; $z/b = 0.0$.

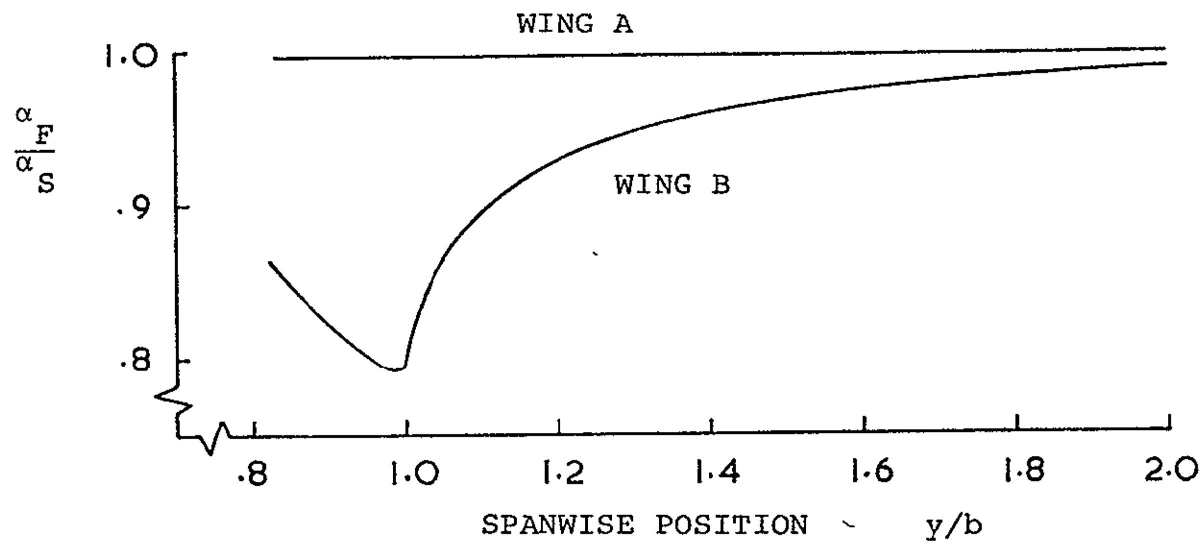

(b) Incidence Ratio.

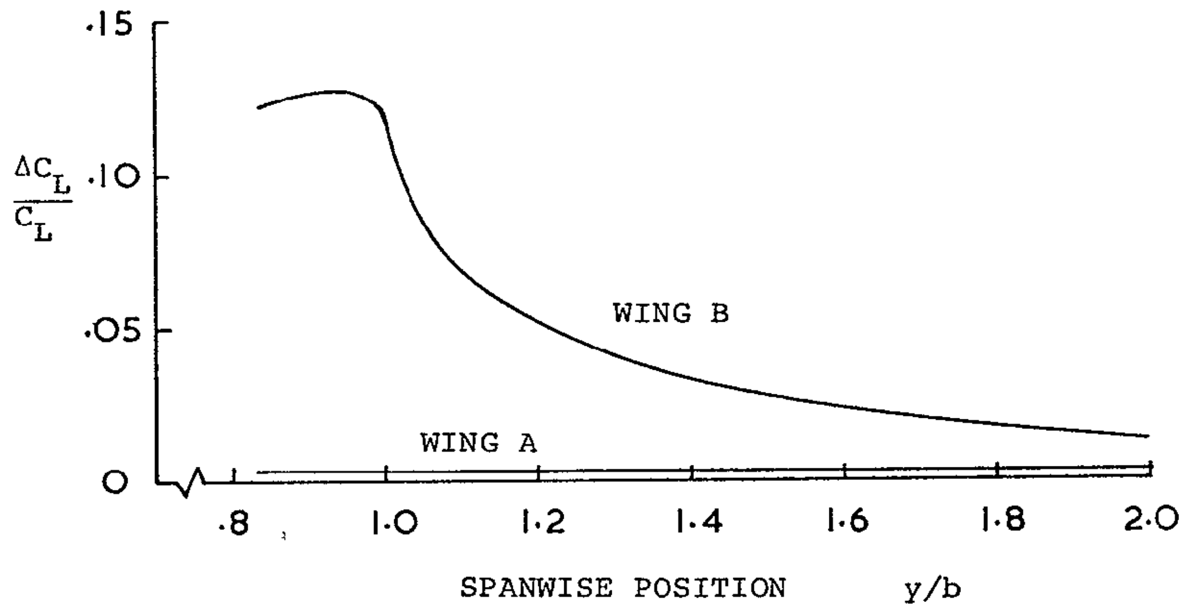

(c) Lift Increment in Formation.

Figure 5. Continued.

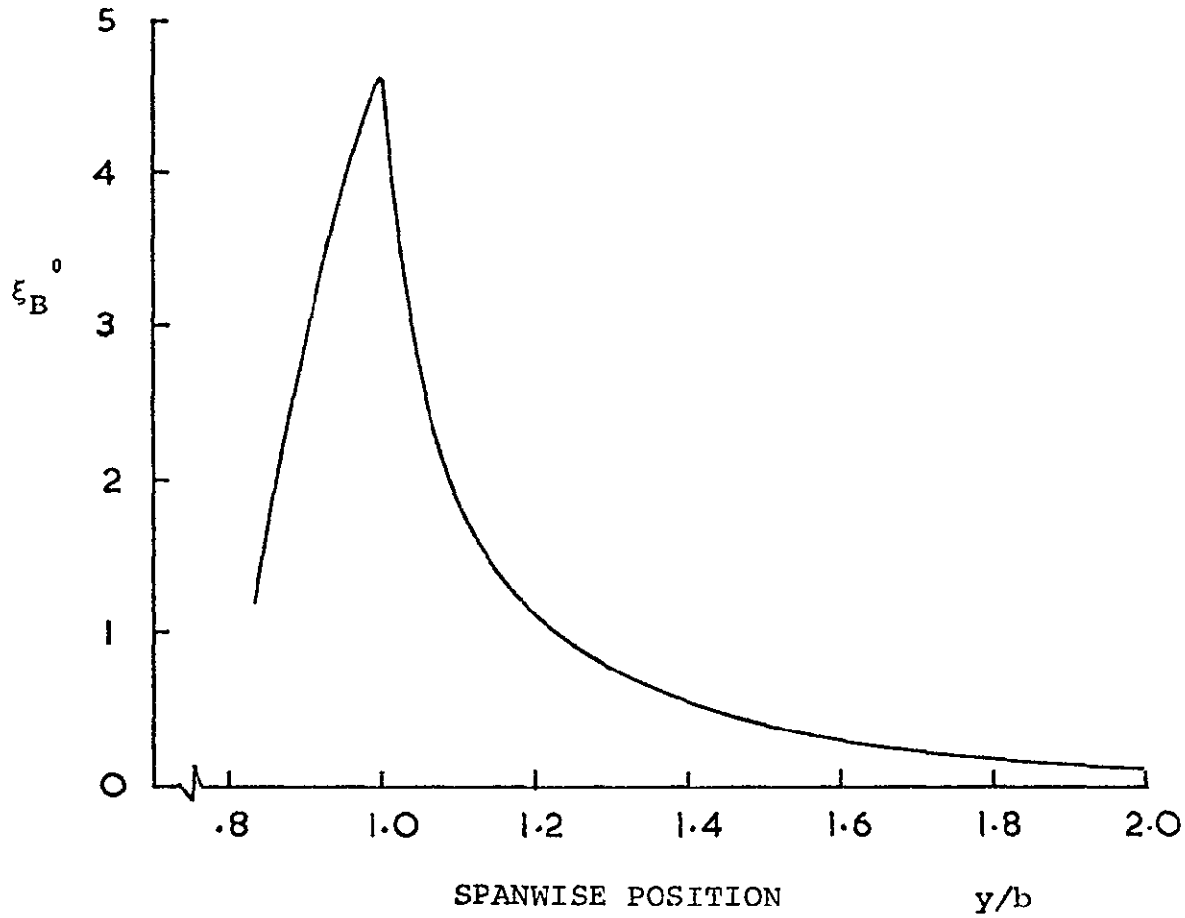

(d) Flaperon Deflection.

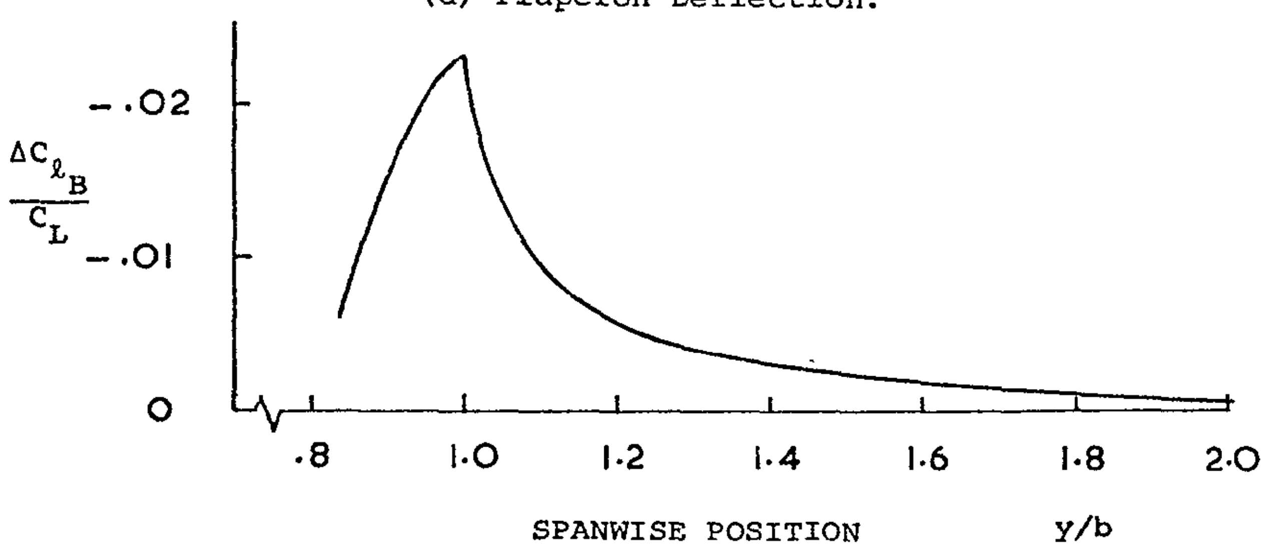

(e) Rolling Moment Increment in Formation.

Figure 5. Concluded.

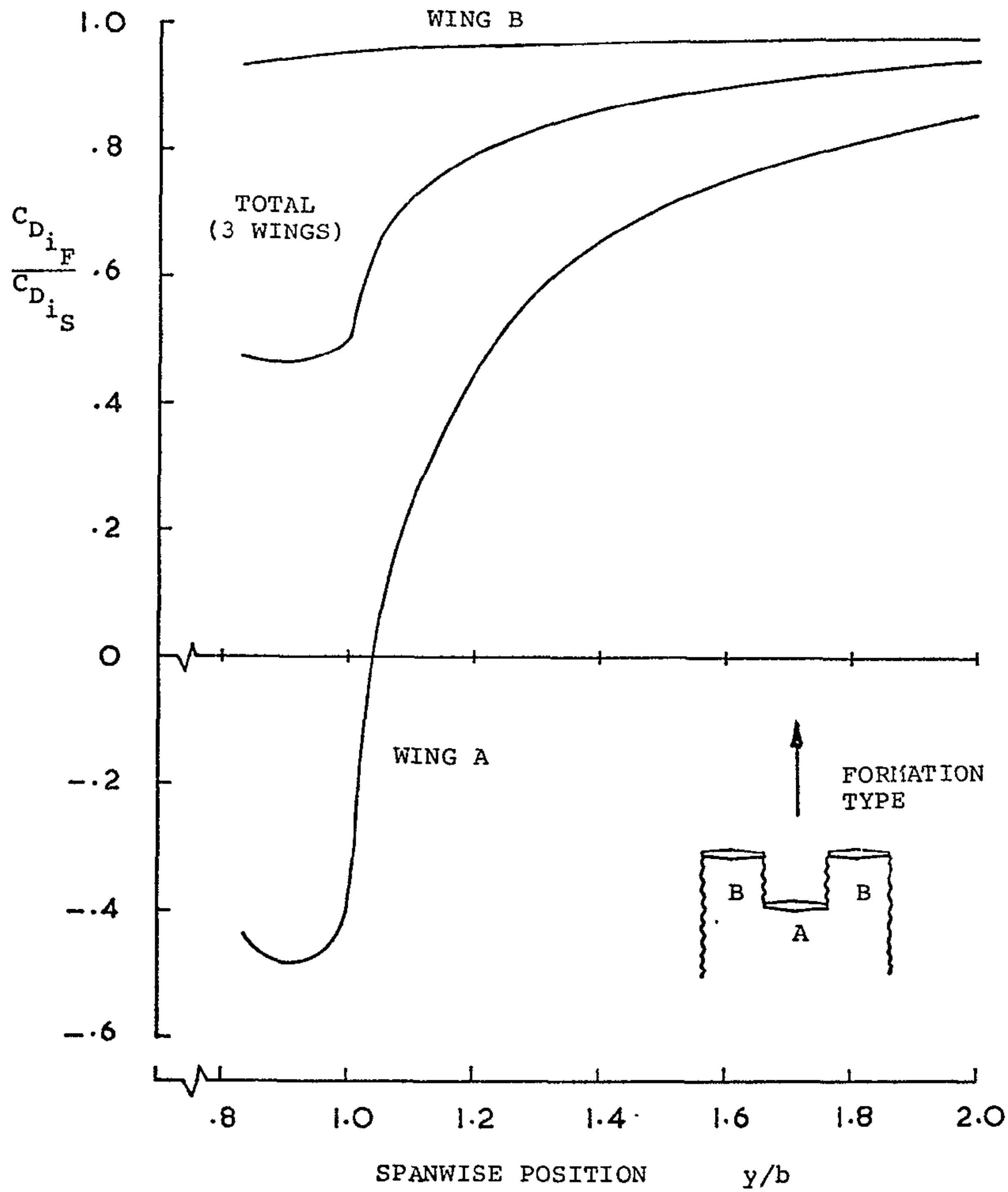

(a) Induced Drag Ratio.

Figure 6. Effect of Spanwise Position: $x/b = -3$; $z/b = 0.0$.

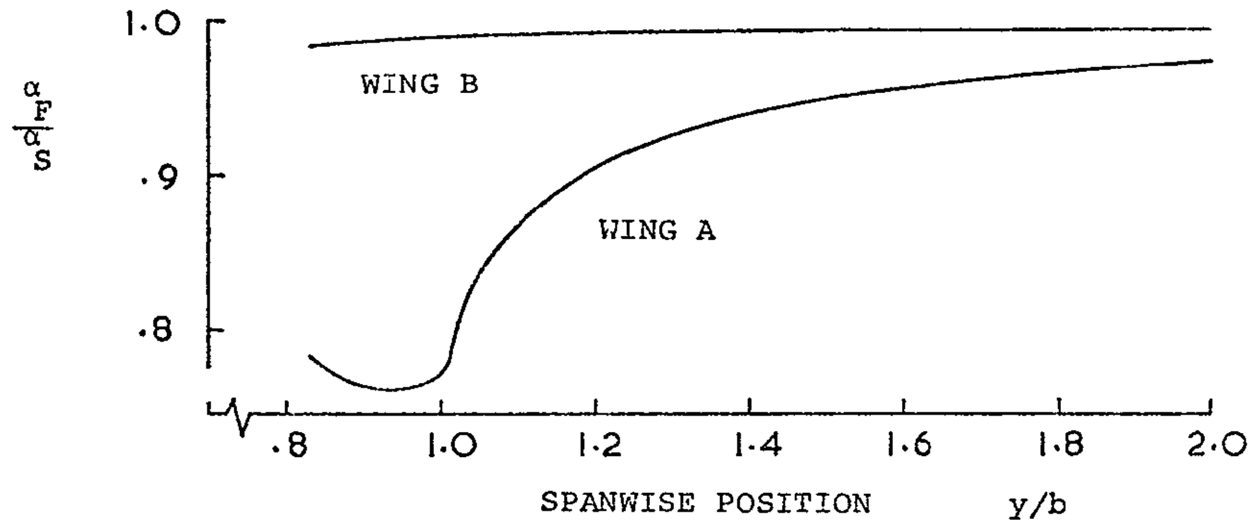

(b) Incidence Ratio.

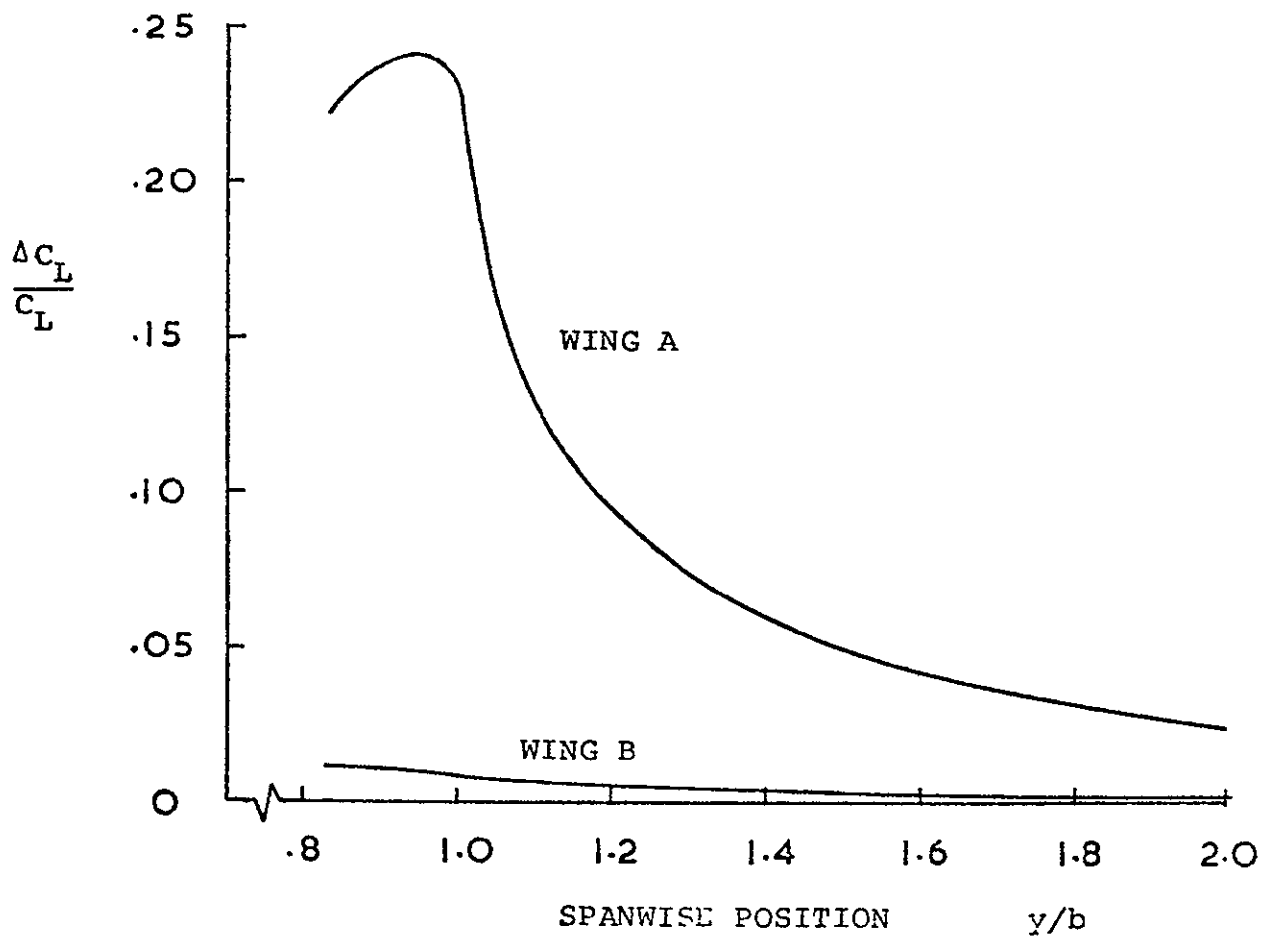

(c) Lift Increment in Formation.

Figure 6. Concluded.

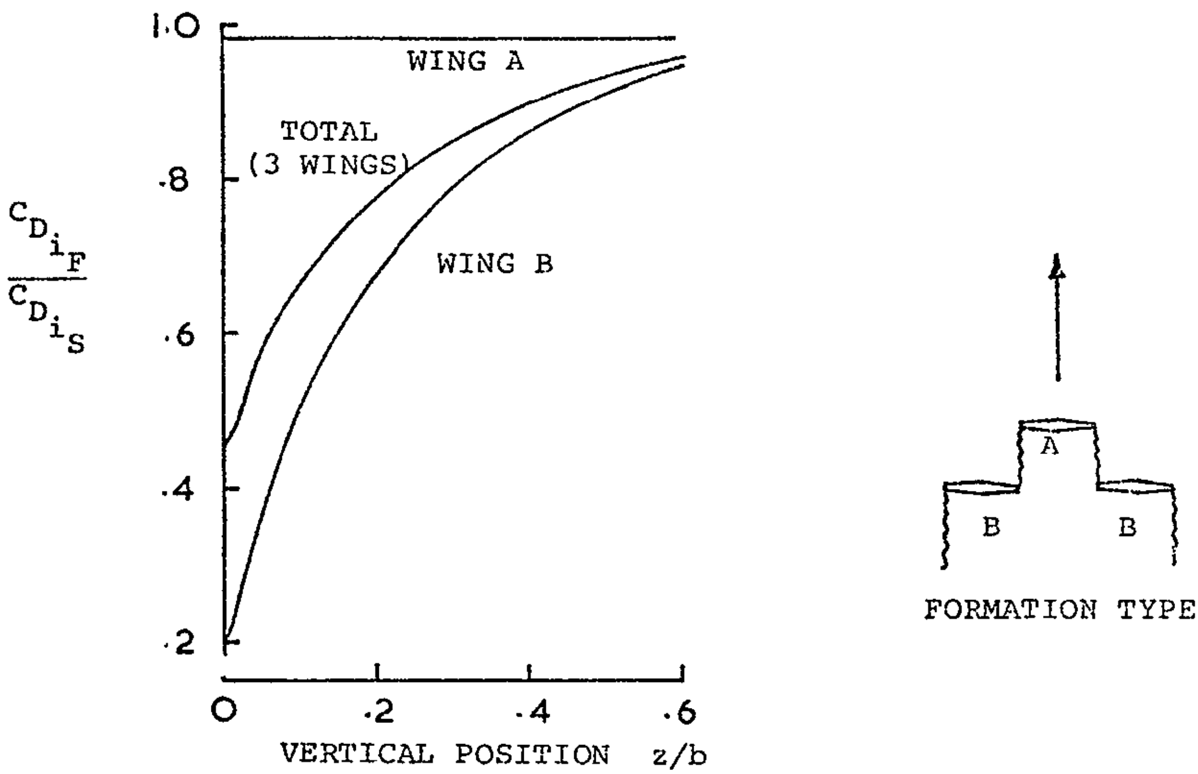

(a) Induced Drag Ratio.

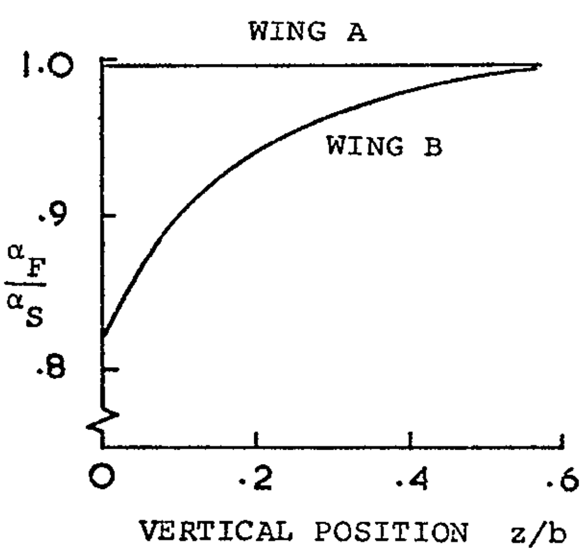

(b) Incidence Ratio.

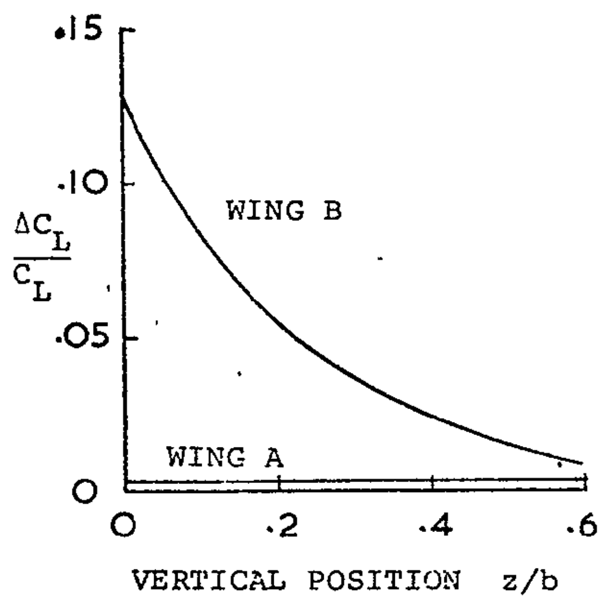

(c) Lift Increment in Formation.

Figure 7. Effect of Vertical Position: $x/b = 3$; $y/b = .89$.

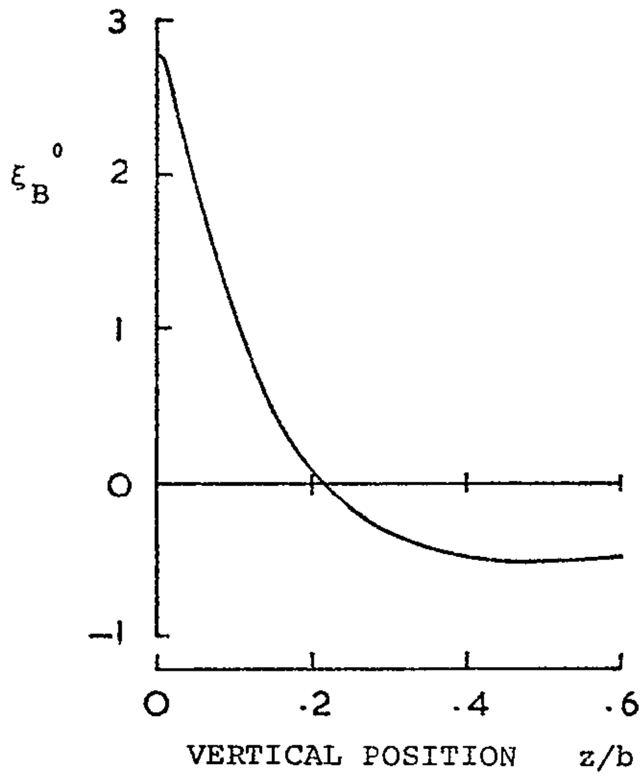

(d) Flaperon Deflection.

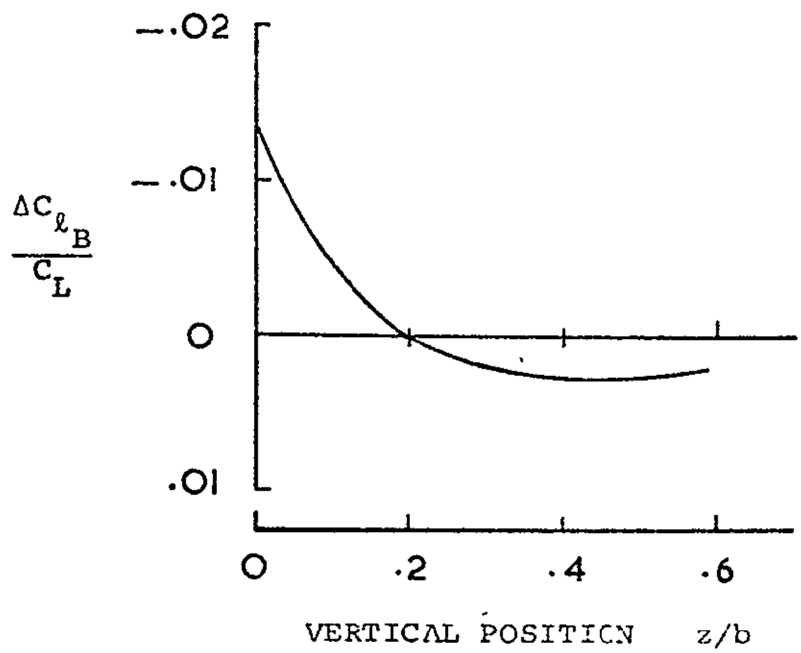

(e) Rolling Moment Increment in Formation

Figure 7. Concluded.

The effect of vertical position on flaperon deflection is shown in figure 7(d). A vertical movement of 0.05b from z = 0 causes a reduction in rolling moment from $-.0134C_L$ to $-.0085C_L$, (fig. 7(e)). In fact, the induced rolling moment changes sign (goes positive) above a z/b value of about 0.2 before returning towards zero. This is because the position of maximum vertical induced velocity on wing B moves outboard as wing B moves vertically; whereas the inner tip of wing B receives the maximum upwash on the wing when z/b = 0, the upwash there rapidly goes toward zero as the tip moves above wing A's trailing vortex sheet.

The results for the vertical scan at x/b = -3 are shown in figure 8. In this case, the results are shown for negative z/b values, i.e., wing A is in the stable lift position above the wakes from wings B. Again, rapid changes with vertical displacement are indicated; a 0.05b vertical movement from z = 0 causes an increase of 0.38 in the induced drag ratio on wing A (fig. 8(a)) while the incidence ratio increases by 0.05 (fig. 8(b)) and the induced lift increment decreases by $0.45C_L$, (fig. 8(c)). The rolling moment for wing B is not presented for this case since it is constant and very small ($\xi_B \simeq 0.1°$).

Effect of Wake Roll-up

In the calculations discussed so far in this Section, the trailing vortex sheet shed by the leading wing (or wings in the case of negative x/b values) is represented by a parallel lattice of semi-infinite vortices. In real flow, the sheet would be almost completely rolled up at three spans downstream, the vortex cores being at the centroid of shed vorticity for each semispan. In the calculations where the lattices overlap (i.e., y/b < 1, see fig. 1), the trailing vortices that pass over the wing induce a downwash over the tip region, whereas they would induce an upwash there if they were at the rolled-up vortex position. Neglecting roll-up, therefore, gives reductions in calculated induced lift and induced thrust; these effects are indicated in the calculated spanwise distributions of lift and induced drag in figure 9(a) and (b), respectively. The calculations discussed so far are, therefore, pessimistic for the maximum induced drag saving, but larger rolling moments would be expected to occur with wake roll-up accounted for.

The loss in induced upwash as the lattices overlap causes the kinks observed in the spanwise scan results at y/b = 1.0 (figs. 5 and 6). Also the turnover in the curves of incidence ratio, induced lift, flaperon angle and induced rolling moment (figs. 5(b), (c), (d), (e) and 6(b) and (c)) would occur at a smaller y/b value as the wing tip passed through the vortex core position.

Two attempts were made to try to allow for the effects of roll-up in the formation with x/b = 3.0 and y/b = 0.89. The first attempt used the iterative vortex roll-up capability of the present calculation method. Several computer runs were carried out, but the calculations were not successful because of the close interaction between the opposing tip vortices and the wing tip. After two iterations, the calculated vortex trajectories passed too close to the following wing control points for reliable force calculations to be made.

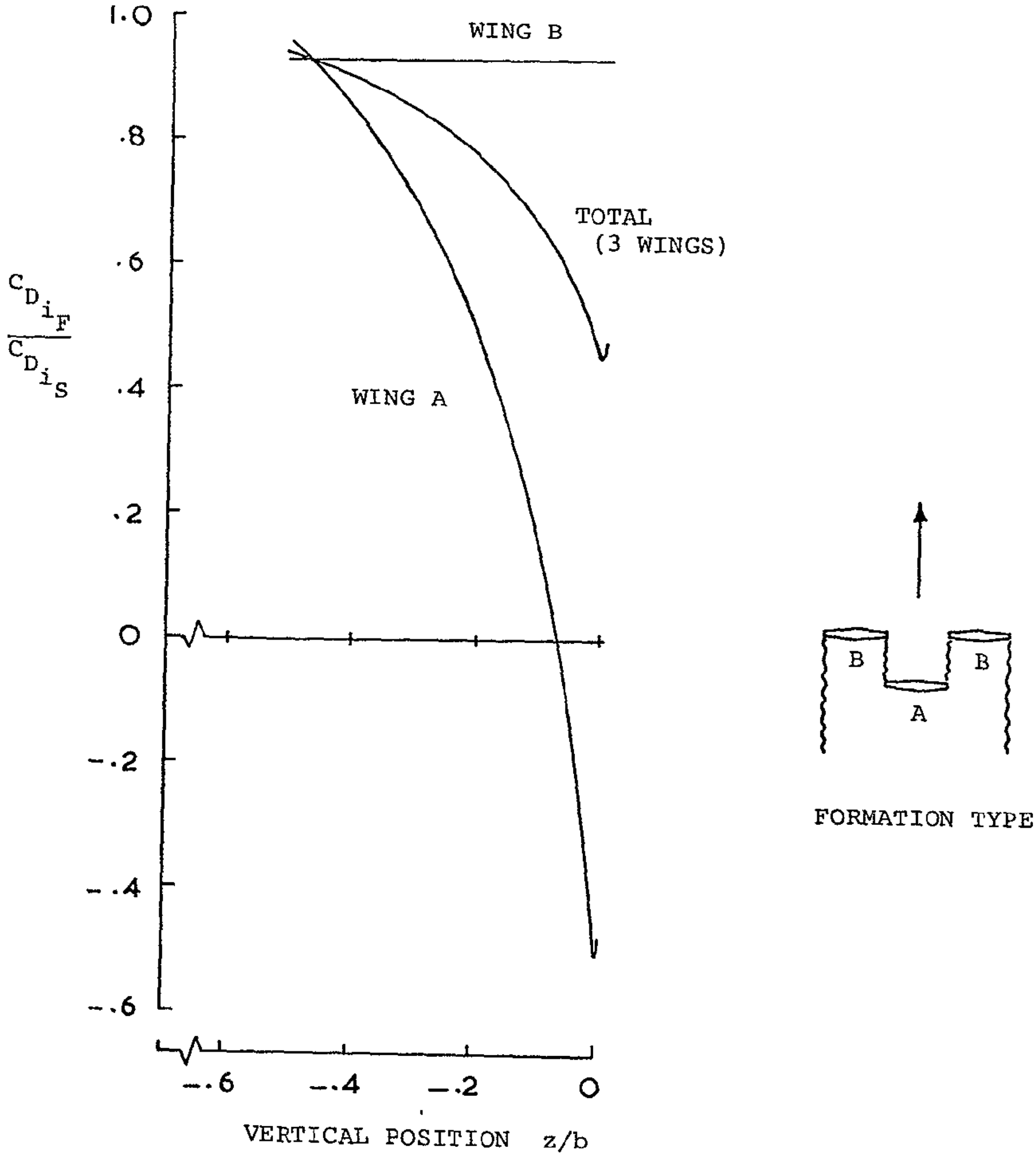

(a) Induced Drag Ratio.

Figure 8. Effect of Vertical Position: $x/b = -3$; $y/b = .89$.

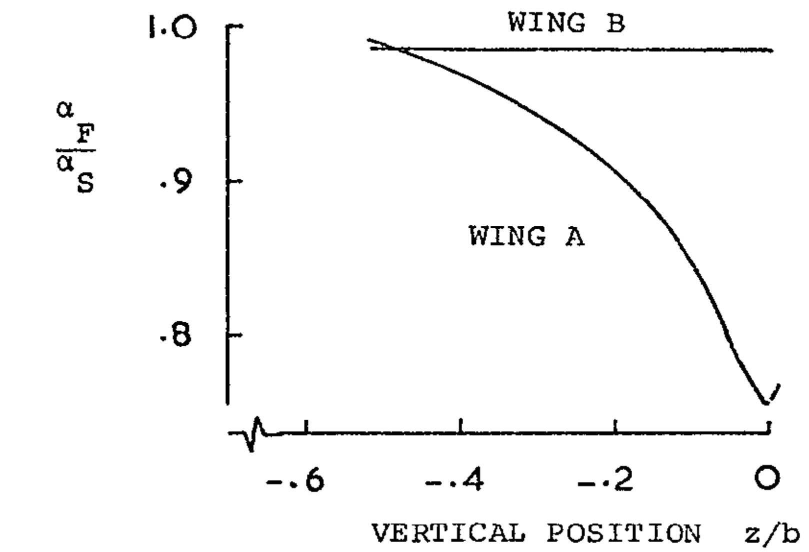

(b) Incidence Ratio.

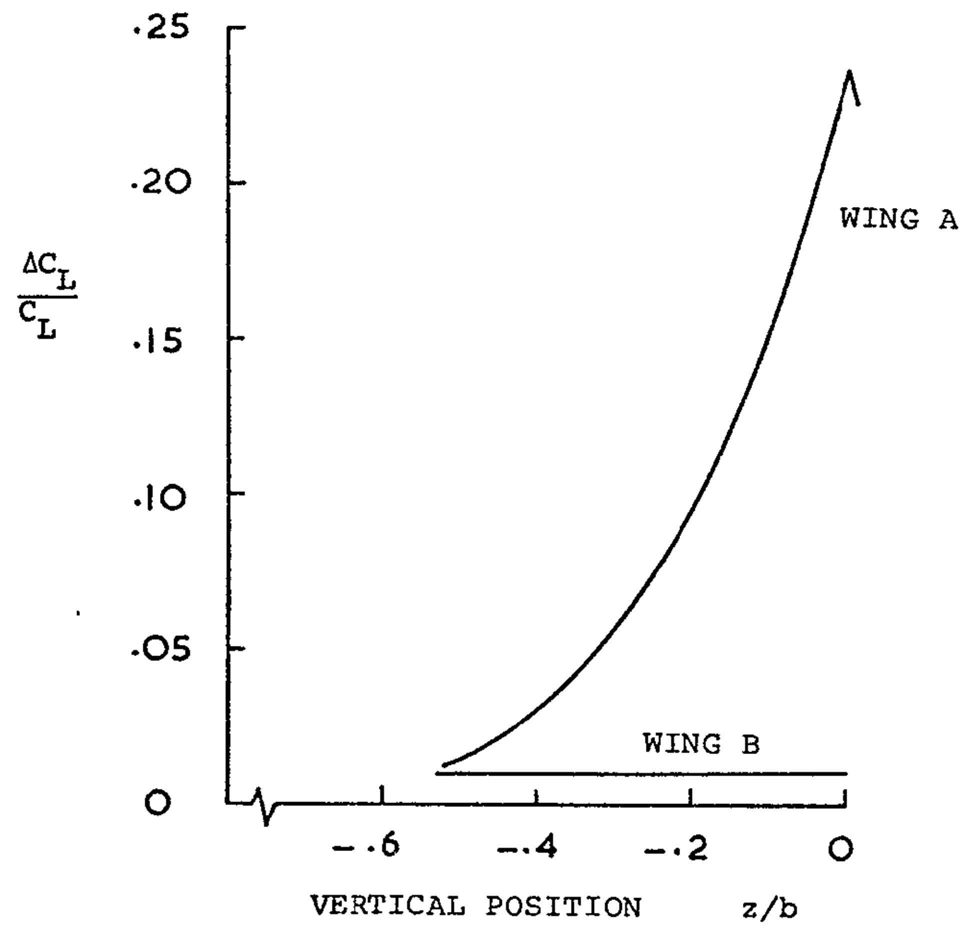

(c) Lift Increment in Formation.

Figure 8. Concluded.

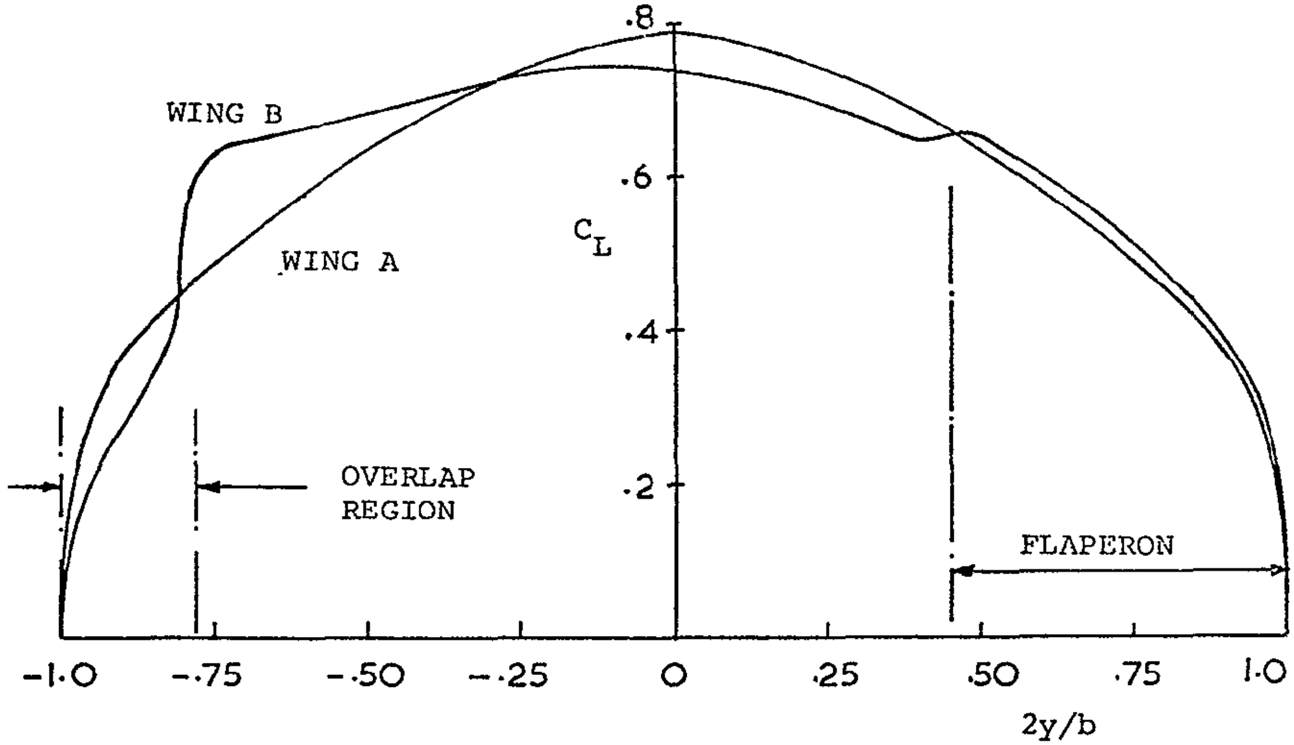

(a) Spanwise Distribution of Lift.

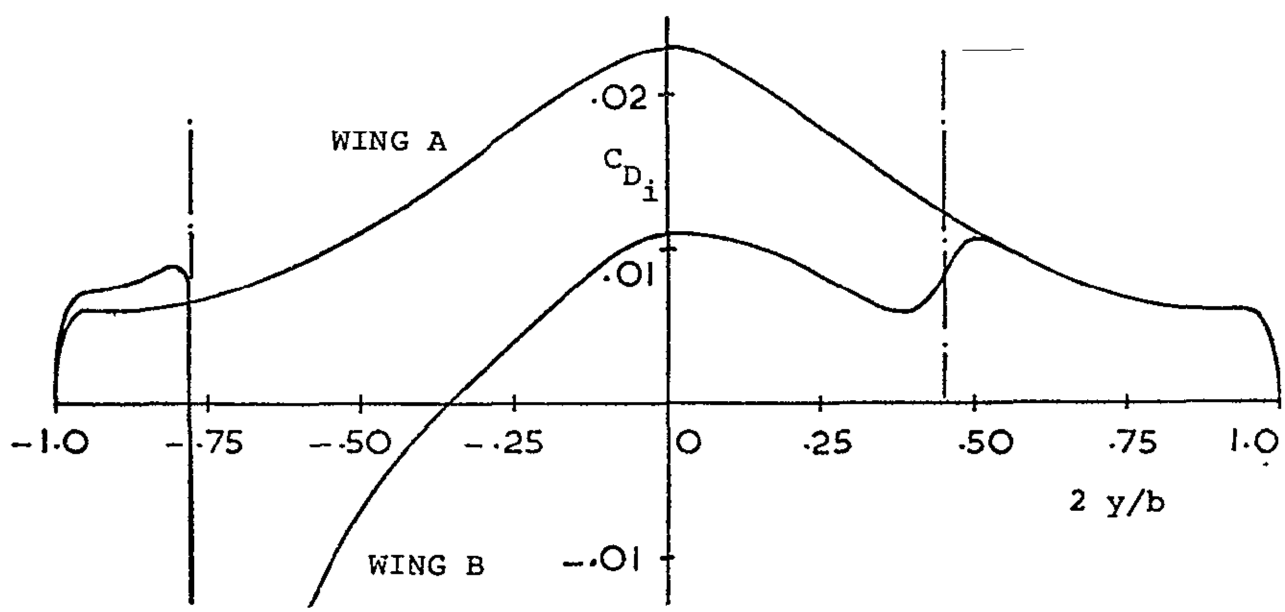

(b) Spanwise Distribution of Induced Drag.

Figure 9. Spanwise Distributions of Lift and Induced Drag: x/b = 3; y/b = .89; z/b = 0.

The problem is essentially a close vortex/wing interaction, and this poses numerical difficulties for a vortex-lattice method. Recent developments in near-field modeling (refs. 7 and 8), would remove these difficulties, but the developments are not yet incorporated in the method.

In a second attempt to allow for wake roll-up, the leading wing and its trailing vortex lattice were replaced by a single vortex having the total circulation of all the trailing vortices on the leading wing semispan. The vortex was placed 0.1b away from the following wing tip. This was done to try to avoid numerical difficulties that occur when calculating the induced thrust on a wing in the presence of a vortex using equation (2) and the vortex-lattice method. Even so, an unduly large induced thrust ratio, -0.62, was calculated.

Further work is clearly required to calculate the effect of roll-up of these formation calculations. Such work should consider near-field modeling techniques such as developed in references 7 and 8.

OPTIMUM FORMATIONS

The present calculations indicate that formation flying with all aircraft having the same induced drag saving is not practical because of the small distances separating the wings. However, comparable savings for the formation as a whole are obtained by having streamwise separation of three or more spans, (fig. 4(a)). This would allow very open formation and should lead to safer operation. With large streamwise spacing, the leading aircraft is essentially in free air, so each aircraft in the formation would take a turn in the lead position to equalize fuel used.

The reason for the improvement in benefit for the following wing as the spacing increases is that the upwash induced by the trailing vortices from the leading wing increases with downstream distance and quickly achieves double the initial value. (In effect, it is the transition from a semi-infinite vortex to an infinite one, and is demonstrated for a single vortex in figure 10.) Wake roll-up would enhance this effect.

Two basic types of open formation appear feasible. The first type is similar to the "V" vormation used by birds, except larger streamwise spacings would be used. The formation could start in echelon (fig. 11(a)), then the leading aircraft could drop back after a time, and so on, until the echelon was reversed. Each aircraft would then have been in the lead position. All the aircraft would require trimming in roll in this formation.

The second type of formation is based on the negative x/b positions, and would have two rows of aircraft. The rows could be swept (fig. 11(b)) to increase the separation between the aircraft in each row. Aircraft in the leading row would have virtually no drag saving, but the second row would achieve double the saving. This type of formation has no basic roll-trim problem, and could be used for ferrying small aircraft. Large, long range aircraft could form the first rows, and each "slot" in between could support several smaller aircraft (e.g., R.P.V.'s) in line astern, (fig. 11(c)). Positions in each "slot" are roll-stable; they are also altitude stable if the following wings are above the level of the trailing vortices.

For the echelon or "V" type of formation, the induced drag ratio for N aircraft would be

$$\frac{C_{D_{i_F}}}{C_{D_{i_S}}} = 0.2 + \frac{0.8}{N} \tag{8}$$

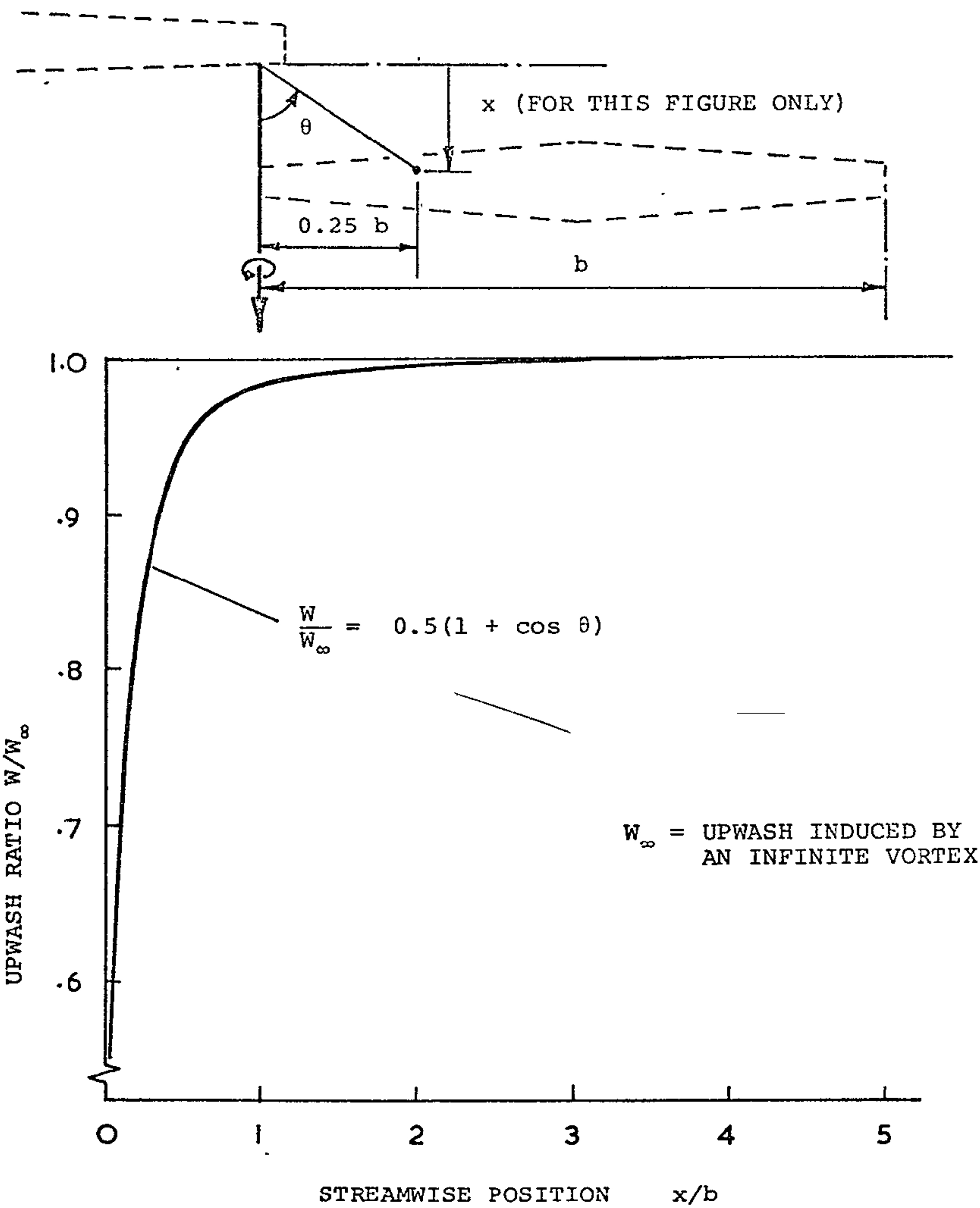

Figure 10. Upwash Induced by a Semi-infinite Vortex.

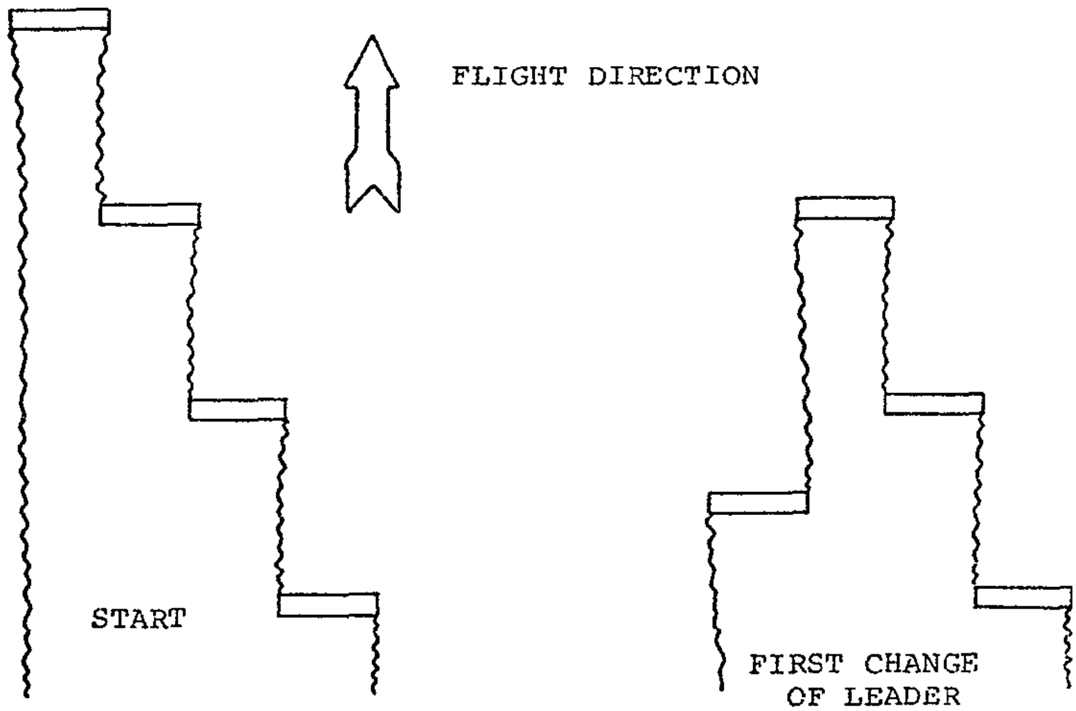

(a) Echelon or "V" Type.

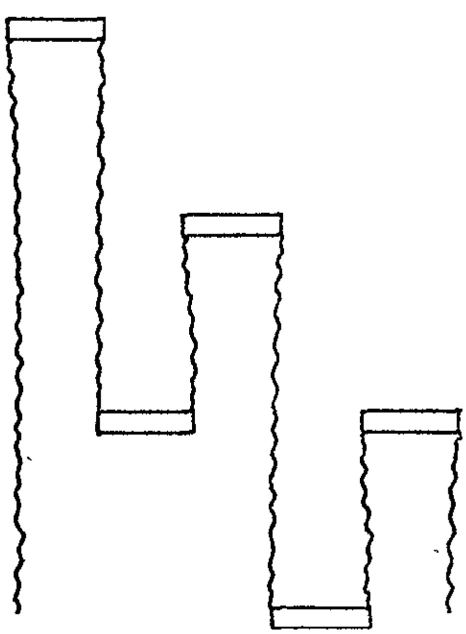

(b) Swept Double Row Type.

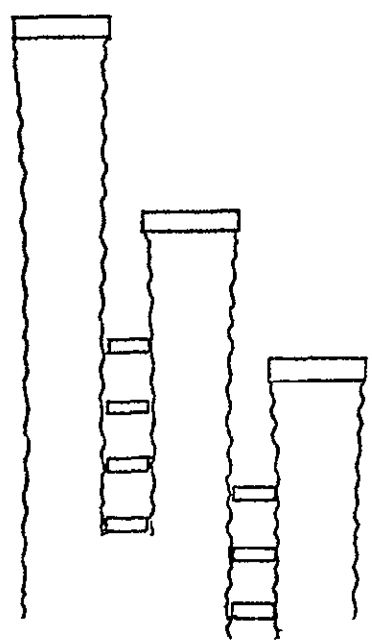

(c) Ferrying Small Aircraft, (e.g., R.P.V.'s).

Figure 11. Possible Formations.

(One leader with no saving and N-1 followers with an induced drag ratio of 0.2.)

For the double row type, the induced drag ratio for N (odd) aircraft would be

$$\frac{C_{D_{i_F}}}{C_{D_{i_S}}} = 0.26 + \frac{0.74}{N} \tag{9}$$

($\frac{(N+1)}{2}$ leaders with no saving and $\frac{(N-1)}{2}$ followers with a thrust ratio of 0.48.)

The induced drag ratio for the double row formation could be reduced by adding an aircraft to each end of the second row. These aircraft would have the 0.2 induced drag-ratio, and would require the trimming in roll.

RANGE EXTENSION

Any general conclusions relative to increase in cruising range which may be expected from reduced induced drag must be approached with caution because factors such as buffet boundaries and drag rise with Mach number are aircraft-dependent. Further, because of lack of simulation and flight experience to assess the feasibility of accurate stationkeeping in formation, it is not known what fraction of the potential reduction in induced drag is achievable under operational conditions. However, automatic stationkeeping using the aircraft automatic flight control system and laser or microwave position determination may be necessary, especially for flights of long duration.

In view of this, it should be recognized that the estimated increases in cruising range using the relationships derived in Appendix A are potential increases, and must be scaled down by some factor depending on the characteristics or constraints of the aircraft considered.

In estimating potential increases in range by flying in formation the following assumptions were made:

* Cruise Mach number is the same in formation flight as for the case of a single aircraft not flying in formation.

* Induced drag can be approximated by the expression

  $C_{D_i} = \left(C_{D_i}/C_L^2\right)C_L^2$, where $\left(C_{D_i}/C_L^2\right)$ is a constant.

* Specific fuel consumption is constant.

* Altitude is allowed to change in order to achieve the desired values of

  C_L/C_D or $C_L^{1/2}/C_D$.

* Mach number effects and buffet boundaries are neglected.

* Zero-lift drag, C_{D_O}, is constant and the same for each aircraft.

* Aircraft in formation change position frequently enough that an average induced drag coefficient, C_{D_i}, can be used for the formation, and each aircraft will consume the same amount of fuel during the mission.

With these assumptions, four formation flight strategies were considered, and estimates were made for range of the formation relative to a range of a single aircraft not flying formation. These four strategies, and the corresponding single-aircraft strategies used for determining relative ranges, are as follows:

A Formation at its max C_L/C_D; single aircraft at its max C_L/C_D.

B Formation at its max $C_L^{1/2}/C_D$; single aircraft at its max $C_L^{1/2}/C_D$.

C Formation flying flight profile similar to that of a single aircraft flying at its max C_L/C_D.

D Formation flying flight profile similar to that of a single aircraft flying at its max $C_L^{1/2}/C_D$.

Equations derived in Appendix A for each of the above cases were used to estimate the relative ranges for each of the above cases, and plotted in the figure below for an echelon formation; double-row formations yield very nearly the same results.

In Figure 12, it can be seen that greatest range increases occur when the formation flies flight profiles optimized for the formation (cases A and B) rather than when the formation flies flight profiles similar to those optimized for an aircraft not flying in formation (cases C and D).

The figure shows significant befit can be derived even for formations of only two aircraft (as much as 30% increase for cases A and B). A point of diminishing return is reached beyond formations of ten aircraft. A reasonable trade-off between a practical formation size and range benefit seems to lie at about three to five aircraft, with corresponding maximum potential range increases of about 46% to 67% (cases A and B). Corresponding increases for case D for three to five aircraft formations are about 15% to 19%. Even these increases could be significant for strategic augmentation missions. Very large formations, say 15 aircraft, show maximum potential increases of about 100%.

Again, a word of caution: it is not known what fraction of this potential range increase is achievable in practice.

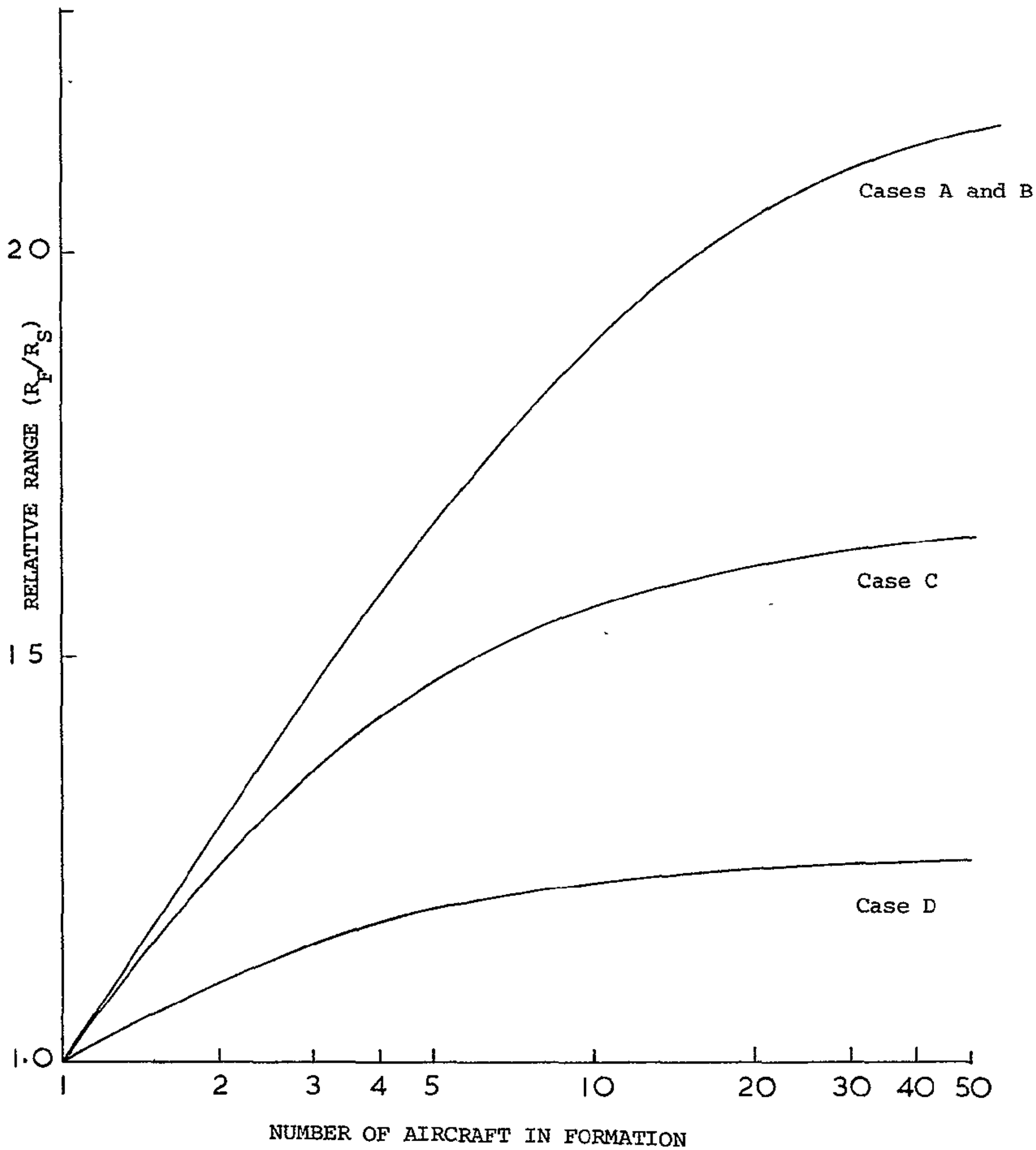

Figure 12. RELATIVE RANGE VS. NUMBER OF AIRCRAFT IN FORMATION
Echelon Formation

CONCLUSIONS AND RECOMMENDATIONS

Conclusions

1) Formations giving equal induced drag saving on all aircraft require dangerously small spacings, but comparable savings for the formation as a whole are obtained with large streamwise spacing. Leading aircraft in the open formations have virtually no induced drag saving.

2) Two types of open formations are possible. The first type is a "V" or echelon type having one leader. Each of the following aircraft would require trimming in roll. The second type of formation has two rows of aircraft. The leading row has virtually no induced drag benefit, but the second row has double the benefit of the echelon type. The second type of formation has no basic out-of-balance rolling moment.

3) Significant induced drag savings are acheived in both formations. Aircraft in the echelon formation have an induced drag of the order of 20% of the free-air value at the same C_L. The second row of the double row formation has an induced thrust of 48% of the free-air induced drag at the same C_L.

4) Both formations are insensitive to longitudinal movements, but benefits (and trimming problems) decrease rapidly with lateral or vertical movements from the optimum position.

5) A reasonable tradeoff between a practical formation size and range benefit seems to lie at about three to five aircraft with corresponding maximum potential range increases of about 46% to 67% with a flight profile optimized for the formation (rather than one optimized for aircraft flying alone). At this time it is not known what fraction of this potential range increase is achievable in practice.

Recommendations

Maximum benefits are obtained when the vortex core from the leader passes close to the tip of the follower. This is a close vortex/wing interaction problem which is beyond the scope of present calculation methods. It is recommended that the numerical problems of calculating close vortex/wing interaction be investigated, based on recent developments in near-field techniques (refs. 7 and 8). Such an investigation should lead to a more accurate assessment of the maximum benefits, and of the sensing and control aspects near the optimum locations.

Additional calculations should be done for different lattice densities. The computer program size limited the number of vortex quadrilaterals for the present calculations. Extensions of the program to allow more quadrilaterals should be considered to investigate the convergence of the results. The method should then be used to assess the range benefits and stability and control aspects of a specific aircraft in formation.

REFERENCES

1. Wieselsberger, C.: Beitrag zur Erklärung des Windkelfluges einiger Zugvögel. Zeitschrift für Flugtechnik und Motorluftschiffahrt, Heft 15, Jahrgang V, August 1914, pp. 225-229.

2. Schlichting, H.: Saving of Power in Formation Flying. Navy Department, The David W. Taylor Model Basin Translation 239, April 1951.

3. Shollenberger, C.A., and Lissaman, P.: Formation Flight of Birds, Science, May 1970.

4. Shollenberger, C.A., and Lissaman, P.: On the Formation Flight of Birds. Unpublished Paper, California Institute of Technology, Circa 1970.

5. Maskew, B.: Numerical Lifting Surface Methods for Calculating the Potential Flow about Wings and Wing-Bodies of Arbitrary Geometry. Ph.D. Thesis, Loughborough University of Technology, England, October 1972.

6. Rubbert, P.E.: Theoretical Characteristics of Arbitrary Wings by a Non-Planar Vortex Lattice Method. D6-9244, The Boeing Company, 1964.

7. Maskew, B.: A Subvortex Technique for the Close Approach to a Discretized Vortex Sheet. NASA TM X-62, 487, 1975.

8. Maskew, B.: A Submerged Singularity Method for Calculating Potential Flow Velocities at Arbitrary Near-Field Points. NASA TM X-73, 115, 1976.

APPENDIX A

DERIVATION OF CRUISING RANGE EQUATION FOR A JET AIRCRAFT

NOTATION:

S = wing area

R = aircraft cruising range, miles

V = true airspeed, MPH

C = specific fuel consumption, lbs. per hour per pound of thrust

L = lift

D = drag

W = aircraft weight

W_B = aircraft weight at beginning of cruise

W_E = aircraft weight at end of cruise

σ = air density at altitude divided by sea level density

ρ = air density

$(\ )_F$ = Denotes formation of aircraft

$(\ )_{FOL}$ = Denotes following aircraft

$(\ )_L$ = Denotes lead aircraft

$(\ )_S$ = Denotes a single aircraft (flying alone)

The purpose of this appendix is to develop some measure of potential range increase which may result from reduction in induced drag due to flying in formation.

It is recognized that the benefits of flying in formation are very much aircraft dependent, and that constraints such as buffet boundaries and drag rise as a function of Mach number together with control problems will probably prevent achieving full potential benefit. However, some generalized computations would still be useful to provide some insight for establishing range performance goals.

A.1 FORMATION CRUISE AT ITS MAXIMUM LIFT-DRAG RATIO

Consider first the case of a single aircraft not flying in formation. Assume that it normally cruises, for maximum range, at a Mach number below the drag rise, perhaps Mach 0.6 to 0.7, and at or near its maximum lift-drag ratio. With these assumptions the cruise altitude will be a function of wing loading (or gross weight, since wing area is fixed).

The classical range equation for jet aircraft is given by the following equation:

$$R = -\int_{W_B}^{W_E} \frac{V}{C} \frac{C_L}{C_D} \frac{dw}{W} \qquad \text{(A-1)}$$

Assume V, C, and C_L/C_D are constant, then

$$R = \frac{V}{C} \frac{C_L}{C_D} \log\,(W_B/W_E) \qquad \text{(A-2)}$$

Now, define relative range as the maximum range of a formation of aircraft divided by the maximum range of a single aircraft. Assuming changes in cruise Mach number, specific fuel consumption and zero-lift drag are negligible, the range of a formation of aircraft at its optimum cruise altitude relative to that of a single aircraft at its optimum cruise altitude becomes:

$$\frac{R_F}{R_S} = (C_L/C_D)_F/(C_L/C_D)_S \tag{A-3}$$

The task now is to determine C_L/C_D for the single aircraft and for the formation. Assuming that the equation for drag coefficient takes the form

$$C_D = C_{D_O} + C_{D_i}$$
$$= C_{D_O} + (C_{D_i}/C_L{}^2)C_L{}^2 \tag{A-4}$$

it can be shown that C_L/C_D is maximum when $C_{D_i} = C_{D_O} = (C_{D_i}/C_L{}^2)C_L{}^2$

The drag coefficient for this condition is then written

$$C_D = 2C_{D_O} = 2(C_{D_i}/C_L{}^2)C_L{}^2$$

And the corresponding lift coefficient is

$$C_L = \frac{C_{D_O}{}^{\frac{1}{2}}}{(C_{D_i}/C_L{}^2)^{\frac{1}{2}}}$$

Subsituting

$$(C_L/C_D)_{max} = \tfrac{1}{2}(C_{D_O}(C_{D_i}/C_L{}^2))^{-\frac{1}{2}} \tag{A-5}$$

Using the subscripts S and F to distinguish the lift-drag ratio for a single aircraft not flying in formation, and for the average of a number of aircraft in formation, respectively, the relative range equation becomes, after substitution for $(C_L/C_D)_{max}$,

$$\frac{R_F}{R_S} = \frac{(C_{D_i}/C_L{}^2)_S{}^{1/2}}{(C_{D_i}/C_L{}^2)_F{}^{1/2}} \tag{A-6}$$

Assuming that the lead aircraft in the formation derive no change in induced drag from the follower aircraft, i.e., their aerodynamic characteristics are basically the same as if they were flying as single aircraft, and assuming the formation may contain N_L lead aircraft, N_{FOL} follower aircraft, and N total aircraft (lead plus follower aircraft), the average induced drag coefficient for the formation is given by,

$$C_{D_{i_F}} = \frac{N_L C_{D_{i_L}} + N_{FOL}\ C_{D_{i_{FOL}}}}{N} \tag{A-7}$$

Since the entire formation will fly at the same lift coefficient, and since the drag coefficient of the lead aircraft will be the same as for a single aircraft not flying in formation,

$$(C_{D_i}/C_L{}^2)_F = \frac{N_L\ (C_{D_i}/C_L{}^2)_S + N_{FOL}(C_{D_i}/C_L{}^2)_{FOL}}{N} \tag{A-8}$$

Substituting into Equation A-6,

$$\frac{R_F}{R_S} = \left[\frac{N_L + N_{FOL}(C_{D_i}/C_L{}^2)_{FOL}/(C_{D_i}/C_L{}^2)_S}{N}\right]^{-1/2} \tag{A-9}$$

A.2 FORMATION CRUISE AT ITS MAXIMUM $C_L^{1/2}/C_D$

Recall the range equation (Equation A-1)

$$R = -\int \frac{V}{C}\ \frac{C_L}{C_D}\ \frac{dw}{W}$$

In equilibrium flight

$$V \left[\frac{2\ W}{\rho_o \sigma S C_L}\right]^{1/2} \tag{A-10}$$

Assume specific fuel consumption, C, is constant. Substituting for V in the range equation

$$R = -\frac{1}{C}\int\left(\frac{2W}{\rho_o S\sigma}\right)^{\frac{1}{2}}\frac{C_L^{\frac{1}{2}}}{C_D}\frac{dw}{W} \tag{A-11}$$

If drag can be approximated by the expression $C_D = C_{D_O} + (C_{D_i}/C_L^{\,2})C_L^{\,2}$, the ratio $(C_L^{\frac{1}{2}}/C_D)$ is maximum when

$$C_L = \left[\frac{C_{D_O}}{3(C_{D_i})/C_L 2}\right]^{\frac{1}{2}} \tag{A-12}$$

The corresponding drag coefficient can then be written

$$C_D = (4/3)C_{D_O} \tag{A-13}$$

and, combining equations A-12 and A-13,

$$(C_L^{\frac{1}{2}}/C_D)_{max} = (1/4)\ (3/C_{D_O})^{3/4}\ (C_{D_i}/C_L^{\,2})^{-\frac{1}{4}} \tag{A-14}$$

Assume that as fuel burns the aircraft is allowed to climb at constant angle of attack, i.e., C_L and $(C_L^{\frac{1}{2}})/C_D$ remain constant, and that cruise Mach number and velocity remain constant. This being the case W/σ is constant and

$$R = \frac{1}{C}\left(\frac{S}{\rho_o S}\frac{W_B}{\sigma_B}\right)\ (C_L^{\frac{1}{2}}/C_D)\ \log\ (W_B/W_E) \tag{A-15}$$

Range of a formation of aircraft relative to a single aircraft then becomes

$$R_F/R_S = (\sigma_{B_S}/\sigma_{B_F})^{\frac{1}{2}}((C_L^{\frac{1}{2}}/C_D)_F/(C_L^{\frac{1}{2}}/C_D)_S) \tag{A-16}$$

$\sigma_{B_S}/\sigma_{B_F}$ is determined from the relationship

$$W_B = \tfrac{1}{2}\rho_o V^2\sigma_B C_L \tag{A-17}$$

If V is essentially the same in going from single aircraft flight to formation flight

$$(\sigma_B C_L)_F = (\sigma_B C_L)_S$$

and

$$\sigma_{B_S}/\sigma_{B_F} = C_{L_F}/C_{L_S} \tag{A-18}$$

Recall that for maximum $C_L^{\frac{1}{2}}/C_D$

$$C_L = \left[\frac{C_{D_0}}{3(C_{D_i}/C_L^{\,2})}\right]$$

Then

$$\frac{\sigma_{B_S}}{\sigma_{B_F}} = \frac{(C_{D_i}/C_L^{\,2})_S^{\frac{1}{2}}}{(C_{D_i}/C_L^{\,2})_F^{\frac{1}{2}}} \tag{A-19}$$

Substituting expressions for $C_L^{\frac{1}{2}}/C_D$ and $\sigma_{B_S}/\sigma_{B_F}$ into the relative range (Equation (A-16),

$$\frac{R_F}{R_S} = \frac{(C_{D_i}/C_L^{\,2})_S^{\frac{1}{2}}}{(C_{D_i}/C_L^{\,2})_F^{\frac{1}{2}}} \tag{A-20}$$

Interestingly, the relative range obtained by maximizing $C_L^{\frac{1}{2}}/C_D$ is the same as that obtained by flying maximum C_L/C_D, and the relative range for the formation can again be written $\frac{R_F}{R_S} = \left[\frac{N_L + N_{FOL}\ (C_{D_i}/C_L^{\,2})_{FOL}/(C_{D_i}/C_L^{\,2})_S}{N}\right]^{-\frac{1}{2}}$ (A-21)

A.3 FORMATION CRUISE PROFILE SIMILAR TO THAT OF A SINGLE AIRCRAFT FLYING AT ITS MAXIMUM LIFT DRAG RATIO

Assume that a single aircraft not flying in formation flies at a maximum, constant lift-drag ratio, and that the formation flies a flight profile similar to that of a single aircraft not flying in formation. This means that the range of the formation relative to that of an aircraft flying single at its maximum lift-drag ratio can be expressed as follows:

$$\frac{R_F}{R_S} = C_{D_S}/C_{D_F}$$
$$= (C_{D_0} + C_{D_{i_S}})/(C_{D_0} + C_{D_{i_F}})$$

$$\frac{R_F}{R_S} = \frac{1 + C_{D_{i_s}}/C_{D_0}}{1 + C_{D_{i_F}}/C_{D_0}} \quad . \tag{A-22}$$

For maximum lift-drag ratio (single aircraft), $C_{D_{iS}} = C_{D_0}$

Hence,

$$R_F/R_S = \frac{2}{1 + (C_{D_{i_F}}/C_{D_{i_S}})} \quad . \tag{A-23}$$

Assuming that C_{D_i} can be approximated by $C_{D_i} = (C_{D_i}/C_L^{\ 2})C_L^{\ 2}$ and that, because the flight profile of the formation is assumed to be similar to that of a single aircraft, the lift coefficients are the same, then

$$\frac{R_F}{R_S} = \frac{2}{1 + (C_{D_i}/C_L^{\ 2})_F/(C_{D_i}/C_L^{\ 2})_S} \tag{A-24}$$

A.4 FORMATION CRUISE PROFILE SIMILAR TO THAT OF A SINGLE AIRCRAFT FLYING AT ITS MAXIMUM $C_L^{1/2}/C_D$

By analogue to the case of a formation cruise profile similar to that of a single aircraft programmed to fly at a constant, maximum C_L/C_D, relative range for flight at maximum $C_L^{\ 1/2}/C_D$ can also be written

$$\frac{R_F}{R_S} = \frac{1 + C_{D_{i_S}}/C_{D_0}}{1 + C_{D_{i_F}}/C_{D_0}} \tag{A-25}$$

From Equation A-13, for maximum $C_L^{1/2}/C_D$,

$C_D = 4/3\ C_{D_O}$

Writing
$$C_{D_{i_S}} = 1/3\ C_{D_O} \quad \text{(a)}$$
$$C_{D_O} = 3\ C_{D_{i_s}} \quad \text{(b)}$$
$$C_{D_{i_F}} = (C_{D_i}/C_L^{\,2})_F C_L^{\,2} \quad \text{(c)} \qquad \text{(A-26)}$$
$$C_{D_{i_s}} = (C_{D_i}/C_L^{\,2})_S\ C_L^{\,2} \quad \text{(d)}$$

and substituting into Equation A-24

$$\frac{R_F}{R_S} = \frac{4/3}{1 + (1/3)(C_{D_i}/C_L 2)_F/(C_{D_i}/C_L 2)_S} \qquad \text{(A-27)}$$

RECAP

The equations derived in this appendix are summarized below for convenience and comparison. Assumptions made in deriving them are:

Specific fuel consumption is constant.

Velocity and Mach number are constant and the same for formation and single aircraft flight.

Altitude is allowed to change to achieve the desired value of $C_L^{\frac{1}{2}}/C_D$ or $C_L^{\frac{1}{2}}/C_D$.

Change in sound velocity with altitude is neglected.

Mach number effects and buffet boundaries are neglected.

Induced drag can be approximated by the expression $C_{D_i} = (C_{D_i}/C_L^2)C_L^2$, where (C_{D_i}/C_L^2) is a constant.

Profile drag, C_{D_O}, is constant and the same for each aircraft.

Induced drag of the lead aircraft of the formation is not affected by other aircraft in the formation; follower aircraft do experience changes in induced drag from aircraft immediately preceding.

AVERAGE INDUCED DRAG COEFFICIENT FOR A FORMATION OF AIRCRAFT WITH N_L LEADERS AND N_{FOL} FOLLOWERS

$$C_{D_{i_F}} = \frac{N_L\ C_{D_{i_L}} + N_{FOL}\ C_{D_{i_{FOL}}}}{N},$$

$$(C_{D_i}/C_L^{\,2})_F = \frac{N_L\ (C_{D_i}/C_L^{\,2})_L + N_{FOL}\ (C_{D_i}/C_L^{\,2})_{FOL}}{N} \qquad \text{(A-28)}$$

Assuming $C_{D_i} = (C_{D_i}/C_L^{\,2})\ C_L^{\,2}$, and $C_{D_{i_L}} = C_{D_{i_S}}$, then

$$\frac{(C_{D_i}/C_L^{\,2})_F}{(C_{D_i}/C_L^{\,2})_S} = \frac{N_L + N_{FOL}\ (C_{D_i}/C_L^{\,2})_{FOL}/(C_{D_i}/C_L^{\,2})_S}{N} \qquad \text{(A-29)}$$

RANGE OF A FORMATION CRUISING AT ITS MAXIMUM FORMATION LIFT-DRAG RATIO RELATIVE TO THAT OF A SINGLE AIRCRAFT FLYING AT ITS MAXIMUM LIFT-DRAG RATIO

$$\frac{R_F}{R_S} = \frac{(C_{D_i}/C_L^{\,2})_S^{\,1/2}}{(C_{D_i}/C_L^{\,2})_F^{\,1/2}} \qquad \text{(A-30)}$$

RANGE OF A FORMATION CRUISING AT ITS MAXIMUM $C_L^{1/2}/C_D$ RELATIVE TO THAT OF A SINGLE AIRCRAFT FLYING AT ITS MAXIMUM $C_L^{1/2}/C_D$

$$\frac{R_F}{R_S} = \frac{(C_{D_i}/C_L^{\,2})_S^{\,1/2}}{(C_{D_i}/C_L^{\,2})_F^{\,1/2}} \qquad \text{(A-31)}$$

RANGE OF A FORMATION FLYING A CRUISE PROFILE SIMULAR TO THAT OF A SINGLE AIRCRAFT FLYING AT ITS MAX C_L/C_D

$$\frac{R_F}{R_S} = \frac{2}{1 + (C_{D_i}/C_L{}^2)_F/(C_{D_i}/C_L{}^2)_S} \qquad \text{(A-32)}$$

RANGE OF A FORMATION FLYING A FLIGHT PROFILE SIMILAR TO THAT OF A SINGLE AIRCRAFT FLYING AT ITS MAX $C_L^{1/2}/C_D$

$$\frac{R_F}{R_S} = \frac{4/3}{1 + (1/3)(C_{D_i}/C_L{}^2)_F/(C_{D_i}/C_L{}^2)_S} \qquad \text{(A-33)}$$

NUMERICAL EXAMPLES

Representative values obtained from Section 5 for use in estimating relative range potential are as follows:

	FORMATION	
	ECHELON	DOUBLE ROW
$C_{D_{i_{FOL}}}/C_{D_{i_S}}$	0.2	-0.48

Substitution of these values into Equations A-27 through A-32 yields the results summarized in Table A-1. Some comments on these results are as follows:

- Echelon formations provide slightly greater benefits than double row formations.

- Relative ranges are significantly greater for formations cruising at flight conditions optimized for maximizing range of the formation (cases A and B in Table A-1) rather then flying flight profiles optimized for maximizing range of a single aircraft.

- Potential cruising range for a formation of five aircraft in estimated to be 67 per cent greater than that of a single aircraft. Constraints, such as buffet boundaries, and possible difficulties in stationkeeping control would probably reduce this potential benefit substantially.

N	R_F/R_S							
	ECHELON FORMATION				DOUBLE ROW FORMATION			
	$\dfrac{(\frac{C_{D_i}}{C_L^2})_F}{(\frac{C_{D_i}}{C_L^2})}$	A & B	C	D	$\dfrac{(\frac{C_{D_i}}{C_L^2})_F}{(\frac{C_{D_i}}{C_L^2})}$	A & B	C	D
1	1.0	1.0	1.0	1.0	1.0	1.0	1.0	1.0
2	.6	1.29	1.25	1.11	.63	1.26	1.23	1.10
3	.467	1.46	1.36	1.15	.507	1.4	1.33	1.14
5	.36	1.67	1.47	1.19	.408	1.57	1.42	1.17
7	.314	1.78	1.52	1.21	.366	1.65	1.46	1.19
9	.298	1.86	1.55	1.22	.342	1.71	1.49	1.20
15	.253	1.99	1.60	1.23	.309	1.80	1.53	1.21
39	.221	2.13	1.64	1.25	.279	1.89	1.56	1.22
99	.208	2.19	1.66	1.25	.267	1.94	1.58	1.22
INFINITE	.20	2.24	1.67	1.25	.26	1.96	1.59	1.23

TABLE A-1. RELATIVE RANGE AS A FUNCTION OF NUMBER OF AIRCRAFT IN FORMATION

A = Formation cruising at max formation C_L/C_D
Single aircraft cruising at its max C_L/C_D.

B = Formation cruising at max formation $C_L^{\frac{1}{2}}/C_D$.
Single aircraft cruising at its max $C_L^{\frac{1}{2}}/C_D$.

C = Single aircraft cruising at its max C_L/C_D.
Formation cruising at single aircraft's max C_L/C_D

D = Single aircraft cruising at its max $C_L^{\frac{1}{2}}/C_D$.
Formation cruising at single aircraft's $C_L^{\frac{1}{2}}/C_D$.